NANOCRYSTALLINE CELLULOSE AND AMORPHOUS CELLULOSE FROM FIBERS OF BANANA WATER HYACINTH AND BAMBOO

PRUTTIPONG PANTAMANATSOPA

A DISSERTATION SUBMITTED IN PARTIAL FULFILLMENT OF THE REQUIREMENTS FOR THE DEGREE OF DOCTOR OF ENGINEERING PROGRAM IN ENERGY AND MATERIALS ENGINEERING FACULTY OF ENGINEERING RAJAMANGALA UNIVERSITY OF TECHNOLOGY THANYABURI ACADEMIC YEAR 2024

NANOCRYSTALLINE CELLULOSE AND AMORPHOUS CELLULOSE FROM FIBERS OF BANANA WATER HYACINTH AND BAMBOO

PRUTTIPONG PANTAMANATSOPA

A DISSERTATION SUBMITTED IN PARTIAL FULFILLMENT OF THE REQUIREMENTS FOR THE DEGREE OF DOCTOR OF ENGINEERING PROGRAM IN ENERGY AND MATERIALS ENGINEERING FACULTY OF ENGINEERING RAJAMANGALA UNIVERSITY OF TECHNOLOGY THANYABURI ACADEMIC YEAR 2024

หัวข้อดุษฎีนิพนธ์ ผลึกนาโนเซลลูโลสและอะมอร์ฟัสเซลลูโลสจากเส้นใยกล้วย ผักตบชวาและไผ่
Nanocrystalline Cellulose and Amorphous Cellulose from Fibers of Banana, Water Hyacinth and Bamboo

ชื่อ – นามสกุล นายพฤติพงศ์ พันธมนัสโสภา

สาขาวิชา วิศวกรรมพลังงานและวัสดุ

อาจารย์ที่ปรึกษา รองศาสตราจารย์วารุณี อริยวิริยะนันท์, D.Eng.

อาจารย์ที่ปรึกษาร่วม ศาสตราจารย์สนอง เอกสิทธิ์, Ph.D.

ปีการศึกษา 2567

คณะกรรมการสอบดุษฎีนิพนธ์

..... ประธานกรรมการ
(รองศาสตราจารย์ถิรายุธ พงศ์ประยูร, ปร.ด.)

..... กรรมการ
(รองศาสตราจารย์วิรชัย โรยนรินทร์, Ph.D.)

..... กรรมการ
(รองศาสตราจารย์สรพงษ์ ภวสุปรีย์, Ph.D.)

..... กรรมการ
(ผู้ช่วยศาสตราจารย์ณรงค์ชัย โอเจริญ, Ph.D.)

..... กรรมการ
(ศาสตราจารย์สนอง เอกสิทธิ์, Ph.D.)

..... กรรมการ
(รองศาสตราจารย์วารุณี อริยวิริยะนันท์, D.Eng.)

คณะวิศวกรรมศาสตร์ มหาวิทยาลัยเทคโนโลยีราชมงคลธัญบุรี อนุมัติดุษฎีนิพนธ์ฉบับนี้เป็นส่วนหนึ่งของการศึกษาตามหลักสูตรปริญญาดุษฎีบัณฑิต

..... คณบดีคณะวิศวกรรมศาสตร์
(รองศาสตราจารย์สรพงษ์ ภวสุปรีย์, Ph.D.)
วันที่ 13 เดือน กุมภาพันธ์ พ.ศ. 2568

Dissertation Title	Nanocrystalline Cellulose and Amorphous Cellulose from Fibers of Banana, Water Hyacinth and Bamboo
Name-Surname	Mr. Pruttipong Pantamanatsopa
Program	Energy and Materials Engineering
Dissertation Advisor	Associate Professor Warunee Ariyawiriyanan, D.Eng.
Dissertation Co-Advisor	Professor Sanong Ekgasit, Ph.D.
Academic Year	2024

ABSTRACT

The growing demand for eco-friendly materials has driven research into new alternative research on using cellulose derived from agricultural waste. This study investigates the synthesis and analysis properties of nanocrystalline cellulose (NCC) and amorphous cellulose (AC) obtained from three agricultural residues: banana trunk fibers (BNNF), water hyacinth (WHF) fibers, and bamboo fibers (BBF) by means of the process of hydrolysis and dissolution in sulfuric acid. The research focuses on optimizing the production conditions and examining the structural properties, morphology and physicochemical properties of the obtained nanocellulose.

The optimized acid hydrolysis conditions gave the highest NCC yields of 68.44% for BNNF, 85.3% for WHF, and 69.46% for BBF, while the acid dissolution conditions gave the highest AC yields of 62.2% for BNNF, 71.6% for WHF, and 65.1% for BBF. Analysis of material properties using techniques XRD, FTIR, SEM and TEM revealed structural differences between NCC and AC. In this regard, NCC showed a high crystallinity index (82.3%-89.5%), which was a result of the efficient removal of amorphous parts by hydrolysis process, and the TEM image showed the appearance of straight rods (whisker-like morphology) with a diameter of 4–20 nm and a length of 50–500 nm. In contrast, AC showed a lower crystallinity index. (26.2%-35.45%) and appeared to be clustered together due to the dissolution of the crystal structure. Furthermore, zeta potential analysis revealed that NCC had significantly better colloidal stability (−30.93 mV to −43.24 mV) compared to AC (−19.73 mV to −17.25 mV), which was due to the formation of charged sulfate ester groups during the acid hydrolysis process. This stability made NCC and AC more suitable for applications that required different stable dispersion in colloidal systems.

This research highlighted the potential upscale of NCC and AC as sustainable materials for biocomposites, biomedical applications and industrial processes. In particular, this study could be considered the first time that bamboo sawdust, banana trunks and water hyacinth have been successfully converted into nanocellulose, demonstrating the feasibility of harnessing these renewable resources to develop green technologies. The research results not only helped solve the environmental problems related to agricultural waste but also paved the way for innovative cellulose applications in sustainable materials development.

Keywords: nanocrystalline cellulose, amorphous cellulose, banana, water hyacinth, bamboo, natural fiber

Acknowledgments

I extend my heartfelt gratitude to my thesis advisor and co-advisor, Associate Professor Warunee Ariyawiriyanan and Professor Dr. Sanong Ekgasit, for their support, invaluable suggestions, motivation, training, and understanding. I am grateful for their patience in guiding and refining my technical skills throughout the entirety of this research journey.

Special appreciation goes to Assoc. Prof. Dr. Yoko Okahisa and the students in her laboratory at Kyoto Institute of Technology, Japan, for welcoming me as an exchange student and generously sharing their technical knowledge and expertise.

I express my sincere appreciation to my thesis committee members: Assoc. Prof. Dr. Thirawudh Pongprayoon, Assoc. Prof. Dr. Sorapong Pavasupree, Asst. Prof. Dr. Narongchai Ojaroen, and Assoc. Prof. Dr. Wirachai Roynarin. Their insightful suggestions, comments, and encouragement have greatly contributed to the development of my thesis.

I would also like to thank my colleagues and everyone at Rajamangala University of Technology Thanyaburi for their valuable suggestions and unwavering support throughout my Ph.D. study. Your collective contributions have been instrumental in shaping the trajectory of my academic journey.

A very special thank you to Dr. Nichanan Phansroy for her constant help and support in every activity throughout my Ph.D. journey. Her willingness to assist at any time has been invaluable to me, and I deeply appreciate her generosity and kindness.

Finally, I would like to thank my parents for all their support.

Pruttipong Pantamanatsopa

Table of Contents

Table of Contents (Continued)

List of Figures

List of Figures (Continued)

List of Figures (Continued)

List of Tables

CHAPTER 1
INTRODUCTION

1.1 Background and Statement of the Problems

Currently, environmental friendliness has emerged as a crucial concern, leading to a rising demand for innovative green materials capable of replacing those derived from fossil resources or synthetic fibers. In this trend, cellulose stands out as a viable option. As the most abundant organic compound on Earth, cellulose offers advantages such as low cost, biodegradability, and low density, making it an intriguing choice for developing novel biomass-based composites [1]. The optimal source of cellulose is cotton due to its cleanliness and high cellulose content (exceeding 90%). However, it is relatively expensive to choose for use. Therefore, in this study, three alternative cellulose sources have been selected: bamboo, banana, and water hyacinth.

Bamboo, a plentiful resource in Thailand, holds the distinction of being the fastest-growing plant on Earth, with certain species achieving an impressive growth rate of up to one meter per day. Playing a crucial role in forest ecosystems, BBF acts as a pioneer species, quickly establishing and enriching soils with humus. Its versatile applications span from traditional hill tribe huts, where it is used for beams, pillars, walls, floors, and roofs, to furniture making, household items, garden tools, scaffolding, raft construction, craftwork, basketry, chopsticks, toothpicks, and paper-making [2]. Despite its myriad uses, each of these processes generates approximately 40% waste, posing a significant challenge for effective waste management.

Banana stands out as a prominent fruit in Thailand, leading in both widespread consumption and the country's agricultural exports. Thailand plays a significant role in the global banana market, supplying substantial quantities to countries like China, Japan, and the Middle East. Bananas are renowned for their versatility in Thai cuisine; bananas are enjoyed as a snack or incorporated into diverse dishes, including fried bananas, banana cakes, and sweet banana desserts. Their adaptability extends to smoothies and fruit salads, contributing flavor and nutritional benefits [3]. Despite their popularity, it's crucial to recognize that the edible part of the banana, the fruit, constitutes only 12% of the plant's total weight, leaving over 80% as agricultural waste. This considerable waste poses

environmental challenges in regions involved in banana farming, emphasizing the need for sustainable waste management practices to foster an eco-friendlier banana industry.

Water hyacinth poses a significant environmental threat in Thailand as an invasive aquatic plant. Recognizable by its vibrant green leaves and captivating purple flowers, it forms dense mats on the water's surface, impeding boat movement, disrupting marine ecosystems, and compromising water quality. This invasive species interferes with multiple human activities, such as transportation, irrigation, and fishing, by clogging waterways and hindering water flow, which is crucial for agriculture. The economic impact extends to communities relying on affected water bodies for livelihoods [4]. Controlling water hyacinths in Thailand presents a formidable challenge. Various methods, including manual removal, biological control employing insects that consume the plant, and herbicides, have been attempted. Despite ongoing efforts to discover sustainable and effective management strategies, the uncontrolled spread of water hyacinth remains a significant issue.

However, three types of agricultural waste, namely BBF, banana, and water hyacinth, present challenges in waste management due to a lack of effective control measures. Current practices, such as storing them for gradual degradation and degradation of plants, have affected the release of gases, including carbon dioxide, contributing to the greenhouse effect. Alternatively, drying and burning these plants results in the greenhouse effect [5] and produces PM2.5 pollutants. However, despite these environmental concerns, a compelling advantage lies in the high cellulose content of these plants, exceeding 60%. This significant cellulose percentage highlights their importance as selected raw materials for produced NCC and AC in this study.

Nanocrystal cellulose (NCC) (some people call cellulose nanocrystals; CNC) represent an intriguing and versatile class of nanomaterials derived from cellulose, showcasing distinctive properties that have garnered significant interest across diverse research and industrial sectors. The advantages of NCC include high strength and stiffness, biodegradability, sustainability, ease of surface chemistry and functionalization, and optical transparency, rendering them applicable in biomedical fields [6]. This unique combination positions NCC as a promising avenue for innovation across various industries. However, historical challenges have limited the efficiency of producing NCC,

with many researchers achieving yields of not more than 40%. Overcoming this efficiency barrier presents a challenge for new researchers to identify optimal conditions in their pursuit of improved production methods.

Amorphous cellulose (AC), distinguished by its absence of a well-defined and ordered crystalline structure, differs from crystalline cellulose, which boasts a highly organized arrangement of cellulose chains. Marked by a more disordered and random configuration of cellulose molecules, AC typically exhibits lower density and mechanical strength than its crystalline counterpart. Yet, its disordered structure imparts greater flexibility and high optical properties. AC finds applications in Biomedical Applications and the Food Industry [7]. Despite its potential, it has attracted comparatively less interest from researchers. Therefore, delving into the study and comparison of AC with NCC becomes an intriguing avenue, holding the promise of introducing additional functionalities to cellulose fibers.

This study focuses on the synthesis and comparison of NCC and AC derived from BBF, banana, and water hyacinth through treatment. The particle size distribution and stability of the resulting nanoparticles were assessed using a particle analyzer. The crystalline structure was examined through X-ray diffraction (XRD). Fourier transform infrared spectroscopy (FTIR) was employed to analyze the chemical structure. The morphology of the samples was investigated using Scanning Electron Microscopy (SEM) and Transmission Electron Microscopy (TEM).

1.2 Objectives

1.2.1 To develop process for preparation of nanofiber from bamboo, banana, and water hyacinth.

1.2.2 To study the effect of temperature on the production of nanofiber.

1.2.3 To characterization of physical properties, morphology, and chemical properties of the nanofiber.

1.3 Scope of this study

1.3.1 Bamboo, banana, and water hyacinth are utilized as raw materials.

1.3.2 Sodium hydroxide is employed in the alkaline treatment process.

1.3.3 Hydrogen peroxide is utilized in the bleaching process.

1.3.4 Sulfuric acid is applied in the acid treatment process.

1.3.5 Morphological, chemical, and crystalline structures of nanocrystal cellulose and amorphous cellulose are characterized using TEM, SEM, FTIR, and XRD.

1.4 Expected output

1.4.1. Identification of optimal conditions for producing nanocrystal cellulose and amorphous cellulose.

1.4.2. Understanding the temperature-dependent control of the structure of nanocrystal cellulose and amorphous cellulose.

1.4.3. Comprehensive characterization of the physical, morphological, and chemical properties of nanocrystal cellulose and amorphous cellulose.

CHAPTER 2
THEORY AND LITERATURE REVIEW

2.1 Raw materials

2.1.1 Bamboo (BBF)

BBF, a versatile and rapidly growing grass of the Poaceae family, is renowned for its multifaceted applications and ecological benefits. Spanning diverse climates worldwide, bamboo stands out as one of the fastest-growing plants, with some species capable of reaching maturity within a few years. The plant's strength-to-weight ratio is comparable to timber, making it an excellent choice for various structural applications, from building materials to furniture and scaffolding. Its unique rhizome-dependent system allows for quick regrowth, contributing to sustainable harvesting practices. Beyond its utilitarian aspects, bamboo holds cultural significance in many societies and plays a vital role in environmental conservation, acting as a carbon sink and providing erosion control. With its remarkable versatility, resilience, and environmental advantages, bamboo continues to gain prominence as a sustainable and renewable resource across diverse industries (Figure 2.1).

Figure 2.1 Bamboo Forest in Prachinburi Province

2.1.2 Banana (BNNF)

BNNF, scientifically classified as members of the genus Musa, are among the world's most widely consumed and economically significant fruits (Figure 2.2). Characterized by their distinctive elongated shape and vibrant yellow peel, BNNF is a rich source of essential nutrients, particularly potassium, vitamin C, and vitamin B6. This versatile fruit is consumed worldwide, either as a convenient and portable snack or as a key ingredient in various culinary applications. BNNF are known for their natural sweetness, providing a quick energy boost, and their creamy texture makes them a popular addition to smoothies, desserts, and breakfast dishes. The BNNF plant, technically a large herb rather than a tree, produces clusters of BNNF known as hands. Interestingly, BNNF are typically harvested while still green and gradually ripening off the plant. Beyond their nutritional value, BNNF plays a crucial role in agriculture and trade, with major BNNF-producing regions located in tropical climates globally.

Figure 2.2 Banana tree in Pathum-Thani province

2.1.3 Water hyacinth (WHF)

WHF (Eichhornia crassipes) is a free-floating aquatic plant known for its rapid growth and expansive green foliage (Figure 2.3). Native to the Amazon basin, WHF has become a widespread invasive species in various regions around the world, particularly in tropical and subtropical climates. Recognizable by its glossy, round leaves and vibrant lavender or violet flowers, WHF often forms dense mats on the surface of freshwater bodies, such as lakes, ponds, and rivers. While aesthetically pleasing, the plant's uncontrolled proliferation can lead to ecological issues, as it hinders sunlight penetration and oxygen exchange, negatively impacting aquatic ecosystems. Despite its invasive nature, WHF has beneficial aspects; its dense root systems can help purify water by absorbing pollutants, and efforts are underway to explore its potential in waste treatment and as a renewable resource for biomass and bioenergy production. Controlling and managing WHF populations remains important to mitigate its ecological impact and harness its potential benefits.

Figure 2.3 Water hyacinth in river in Pathum-Thani province

2.2 Cellulose

Cellulose is a complex carbohydrate that serves as a fundamental building block in the structural framework of plant cells. Composed of linear chains of glucose molecules linked by β-1,4-glycosidic bonds (as shown in Figure 2.4), cellulose molecules align to form microfibrils with a highly organized and crystalline structure. This arrangement imparts remarkable strength and rigidity to plant cell walls, providing structural support to the entire plant. The hydrogen bonds between adjacent cellulose chains contribute to the stability of these microfibrils, creating a robust network that withstands environmental stresses and supports the plant's form.

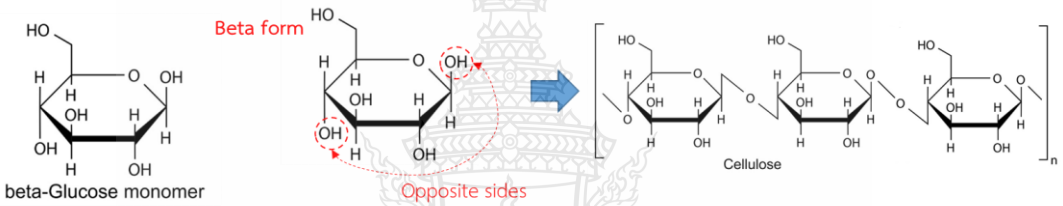

Figure 2.4 Cellulose chains

One distinctive feature of cellulose is its resistance to digestion by most animals, including humans, due to the lack of enzymes capable of breaking the β-1,4-glycosidic bonds. As a result, cellulose functions as an essential dietary fiber. While it does not contribute directly to caloric intake, cellulose plays a crucial role in promoting digestive health by adding bulk to the diet and aiding in the movement of food through the digestive tract. Foods rich in cellulose, such as fruits, vegetables, and whole grains, are often recommended for their positive impact on digestive processes.

Beyond its biological role, cellulose has significant industrial applications. The cellulose extracted from plant sources is a key raw material in the production of paper and textiles. Additionally, cellulose derivatives, such as cellulose acetate and carboxymethyl cellulose, find use in various industries, including food, pharmaceuticals, and cosmetics. As a renewable and abundant biopolymer, cellulose exemplifies the

intersection of biological importance and industrial utility, contributing to both natural processes and human technological advancements.

Cellulose fibers primarily consist of cellulose, along with lignin and hemicellulose. When obtaining pure cellulose from plants is essential, the crucial step is purification, which involves removing lignin, hemicellulose, and other impurities to retain only cellulose. BBF, BNNF, and WHF exhibit higher cellulose content compared to various other agricultural wastes. This elevated cellulose content provides a potential advantage in the production of cellulosic products from agricultural waste. The specific cellulose content values for various agricultural wastes are detailed in Table 2.1.

Table 2.1 Composition of cellulose fibers

Fiber	Hemicellulose	Lignin	Cellulose	Ref.
Cotton	5.7	-	82.7	[8]
Bamboo	12.49	10.15	73.83	[9]
Oil palm	-	19	65.0	[10]
Kenaf	33.9	21.2	53.4	[10]
Banana	19	5-10	60-65	[11]
Water hyacinth	22.3	6.6	67.5	[12]
Sisal	12	9.9	65.8	[8]

2.2.1 Purification of cellulose fiber

The purification of cellulose involves several processes to isolate this essential biopolymer from the complex matrix of plant materials. The first step typically involves harvesting or collecting plant biomass, including BNNF, BBF, WHF, cotton, or other cellulose-rich sources. Once obtained, the raw material undergoes a series of mechanical and chemical treatments to remove impurities such as lignin, hemicellulose, and pectin. Mechanical processes, like milling and grinding, help break down the plant structure and expose cellulose fibers. Subsequent chemical treatments, often involving alkaline solutions, are applied to dissolve or remove non-cellulosic components, leaving behind a cellulose-rich material.

After alkaline treatment, further purification steps are often employed to enhance the purity of cellulose. One standard method is bleaching, which involves treating the cellulose with chemicals like H_2O_2 or chlorine dioxide to remove residual color and any remaining impurities. The resulting purified cellulose can be in the form of pulp, which is then further processed for specific applications. In the paper industry, for instance, purified cellulose is typically refined and formed into sheets for paper production. In textile manufacturing, cotton undergoes additional processes like carding and spinning to produce purified cellulose fibers that are woven into fabrics. Example as shown in Table 2.2

Table 2.2 Literature review for pre-treatment process

Cellulose materials	Purification method		Ref.
	Alkaline treatment	Bleaching	
Water hyacinth	15% (w/w) NaOH at 130 ºC for 6 h	A mixture of $NaClO_2$ and CH_3COOH at 60 ºC for 2h	[13]
Palm oil	2% (w/w) NaOH at 70 ºC for 3 h	Acetate buffer with 1.7% $NaClO_2$ at 80 ºC for 2h	[14]
Banana	2M NaOH at 80 ºC for 2 h	H_2O_2 and CH_3COOH at 70 ºC for 2h	[15]
Bamboo	3% (w/w) NaOH at 50 ºC for 2 h	H_2O_2 at 70 ºC for 2h	[16]
Pineapple leaf	2% (w/w) NaOH at 100 ºC for 4 h	A mixture of $NaClO_2$ and CH_3COOH at 80 ºC for 4h	[17]

Purified cellulose finds diverse applications beyond traditional industries. It is a crucial component in producing cellulose derivatives, such as cellulose acetate and carboxymethyl cellulose, which are utilized in the pharmaceutical, food, and cosmetic industries. The purification of cellulose not only allows for the utilization of its inherent strength and versatility in industrial processes but also plays a vital role in minimizing environmental impact by reducing the need for chemical treatments and optimizing the efficiency of cellulose-derived products.

2.2.2 Cellulosic product

To cater to diverse and advanced applications, cellulose fiber can be manufactured in various types by altering particle size (length and diameter), crystalline structure, surface modification, and colloidal stability.

2.2.2.1 Microcrystalline cellulose (MCC)

MCC is a widely used and versatile excipient in the pharmaceutical and food industries. It is derived from purified cellulose, typically obtained from wood pulp or plant fibers, which undergoes a controlled hydrolysis process. During hydrolysis, the amorphous regions of cellulose are removed, leaving behind fine crystalline particles with a high degree of purity. This results in a white, odorless, and tasteless powder with excellent compressibility and flow properties.

In pharmaceutical formulations, microcrystalline cellulose serves as an essential ingredient in the production of tablets and capsules. Its unique properties, including its ability to act as a binder, disintegrant, and filler, contribute to the cohesion and mechanical strength of tablets while aiding in their disintegration upon ingestion. MCC is biocompatible, inert, and widely accepted by regulatory authorities, making it a preferred choice for formulating oral dosage forms. Additionally, in the food industry, microcrystalline cellulose is used as a bulking agent, anti-caking agent, and texturizer in various food products, providing improved texture and stability. Its versatility and widespread acceptance make microcrystalline cellulose a crucial component in the manufacturing of pharmaceuticals and food products. [1]

2.2.2.2 Cellulose nanofibers (CNF)

CNF are ultrafine fibers derived from cellulose, the main structural component of plant cell walls. These nanofibers typically have diameters in the nanometer range, ranging from 5 to 20 nanometers, and possess exceptional mechanical properties, high aspect ratios, and a large surface area. The production of CNF involves breaking down cellulose fibers through mechanical processes, such as high-pressure homogenization or micro fluidization, to obtain nanoscale dimensions. Alternatively, enzymatic or chemical treatments can be employed to disintegrate cellulose into nano fibrillated structures[18].

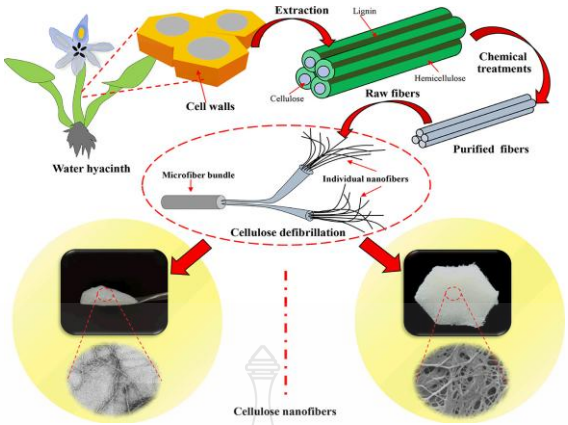

Figure 2.5 A schematic diagram of the cellulose nanofibers. [18]

Due to their unique properties, particularly their small particle size, cellulose nanofibers find applications in various industries, including materials science, electronics, and biomedical engineering. In materials science, CNF are used as reinforcement agents in nanocomposites, enhancing the mechanical strength and structural integrity of materials such as polymers. In the field of electronics, CNF are explored for their potential in flexible and transparent conductive films. Additionally, the biocompatibility and sustainability of cellulose nanofibers make them promising candidates for biomedical applications, such as drug delivery systems and tissue engineering scaffolds. The versatility and eco-friendly nature of cellulose nanofibers contribute to their growing significance in advancing innovative technologies across diverse sectors.

2.2.2.3 Nanocrystal cellulose (NCC) or cellulose nanocrystal (CNC)

NCC are nanoscale particles derived from cellulose, the primary structural component of plant cell walls as shown in Figure 2.6. These NCC are typically obtained through acid hydrolysis, a process that selectively removes the amorphous regions of cellulose, leaving behind highly crystalline and rod-shaped particles with dimensions on the nanometer scale. The resulting NCC usually have diameters ranging from 5 to 20 nm and lengths varying from 100 to 300 nm [19]. This small size imparts unique properties to NCC, including a high surface area-to-volume ratio and excellent dispersibility in various solvents.

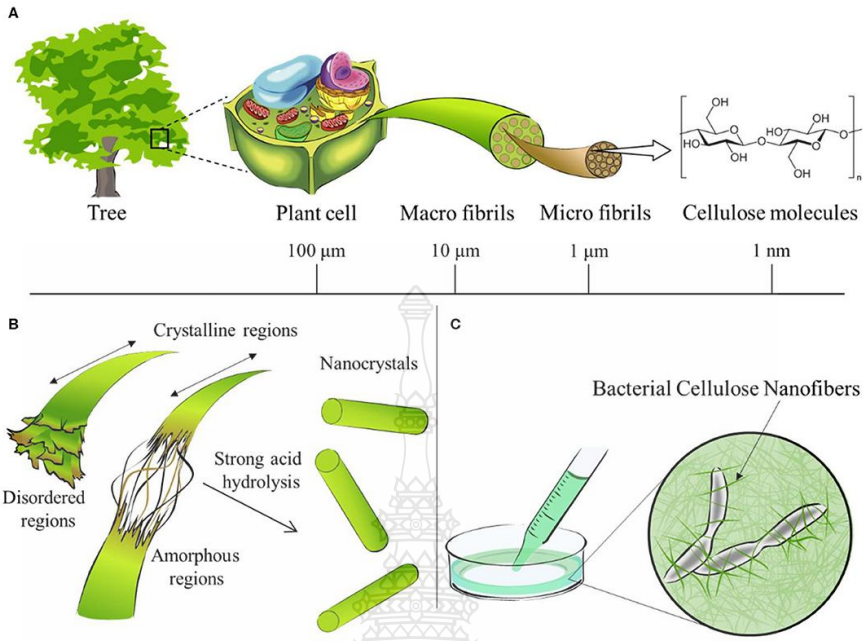

Figure 2.6 A schematic diagram of NCC from plant [19]

NCC possess exceptional mechanical properties, including high tensile strength and stiffness, owing to their well-defined crystalline structure. The high aspect ratio and biocompatibility of NCC contribute to their versatility and applicability across different fields. In materials science, NCC are utilized as reinforcing agents in nanocomposites, contributing to enhanced strength and durability. Their small size and unique characteristics make them promising candidates in biomedical applications, such as drug delivery systems and tissue engineering scaffolds. Additionally, NCC are explored for their potential in creating transparent films, barrier coatings, and as components in renewable and sustainable materials. The eco-friendly nature, nanoscale dimensions, and versatile properties of NCC position them as a promising and sustainable nanomaterial for various innovative and environmentally conscious applications.

2.2.2.4 Amorphous cellulose (AC)

AC refers to the non-crystalline or disordered form of cellulose, a major component of plant cell walls. Unlike the highly organized and crystalline regions found in cellulose, AC lacks a distinct arrangement of cellulose chains.

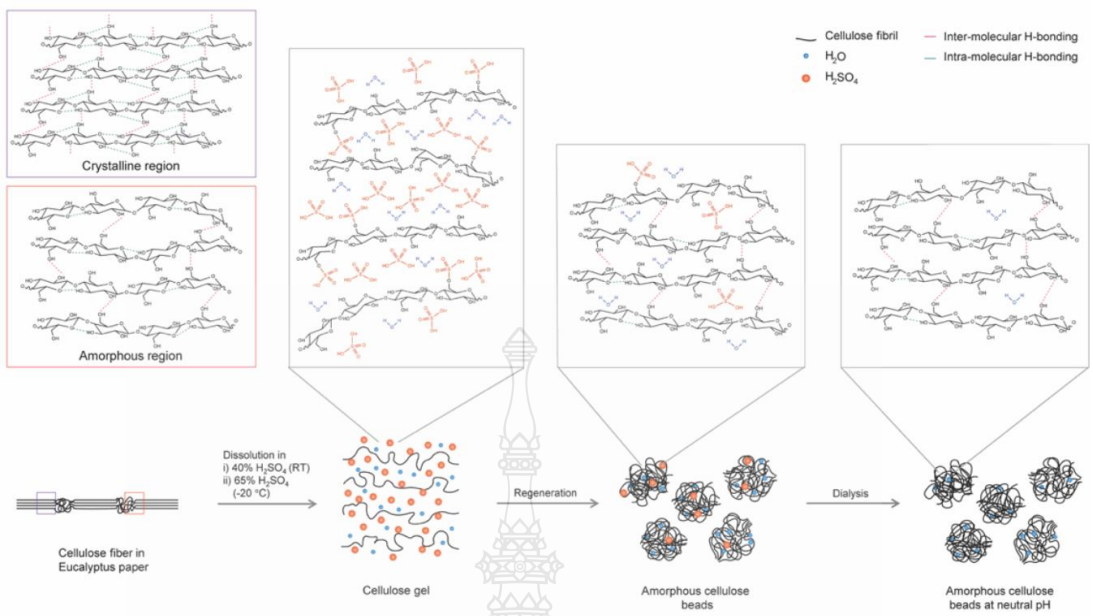

Figure 2.7 Structural transformation of eucalyptus to AC [20]

This amorphous structure arises from various factors, including the presence of impurities, processing conditions during cellulose extraction, and the inherent complexity of plant biomass. AC (Figure 2.7) coexists with crystalline cellulose in the cellulose matrix and plays a crucial role in influencing the solubility, reactivity, and mechanical properties of cellulose in different applications. The particle size of AC, particularly in its nanoscale dimensions, is of interest in various industries. These dimensions can range from a few nanometers to micrometers. The small particle size contributes to the increased surface area, which is significant in applications like drug delivery, where AC nanoparticles may offer improved solubility and controlled release properties. Understanding the particle size distribution of AC is crucial for tailoring its properties in applications such as nanocomposites, biomaterials, and pharmaceutical formulations, where the interplay between NCC and AC influences the material's overall performance. Researchers are actively exploring the unique characteristics of AC particles to unlock their full potential in advancing sustainable materials and biotechnological applications.

2.3 Characterization

2.3.1 Microstructure

In a related study, Tong et al. (2021) [21] investigated the pretreatment of BBF sawdust for reinforcement in cement. Figure 2.8 illustrates morphological changes in BBF particles following different treatments. Untreated particles (Figure 2.8a) display cell walls covered in wax, pectin, and impurities. Cold water treatment (Figure 2.8b) removes impurities, creating a neater surface. Figures 2.8c and 2.8d show cellulose defibrillation, resulting in rougher surfaces. Alkali treatment is more intense than hot water, increasing surface roughness by disrupting hydrogen bonding in the network structure.

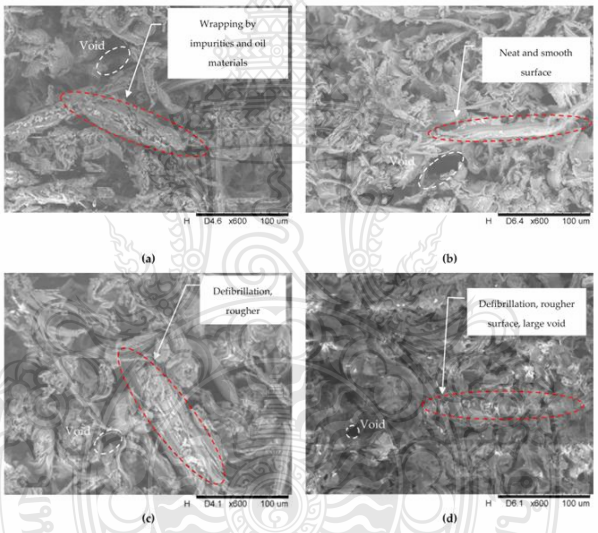

Figure 2.8 SEM image of BBF; (a) without treatment, (b) with aqueous treatment, (c) with hot aqueous treatment and (d) 10% concentration alkali treatment

Soraisham et al. (2022) [22] conducted a study on the pretreatment of BNNF. The microstructure of BNNF fibers (Figure 2.9a) revealed longitudinal ridges and an exceptionally uneven surface with impurities. Chemically bleached fibers not only exhibited a clean and smoother surface but also appeared finer (Figure 2.9b), possibly attributed to the removal of surface gummy materials, promoting individualization.

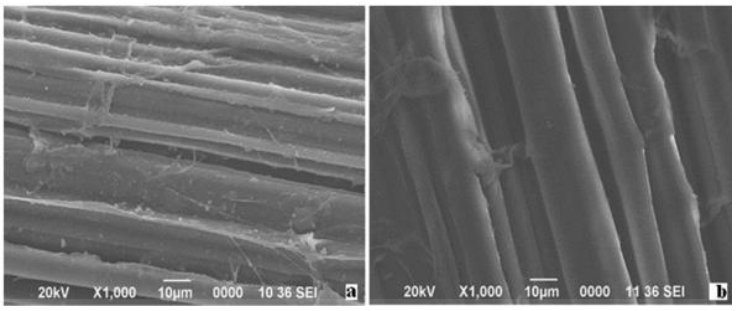

Figure 2.9 SEM image of BNNF fiber; (a) Retted and (b) Bleached.

In 2023, Gorgr et al. [12] conducted a study on extracting fibers from WHF. Figure 2.10 illustrates the surface morphology of WHF fibers. In the retted fibers, the surface appears rough, retaining a slight amount of fleshy materials even after combing and washing. However, following alkali treatment, the surface becomes smooth and devoid of fleshy matters (Figure 2.10c, d). Consequently, a slight reduction in fiber diameter was observed after degumming.

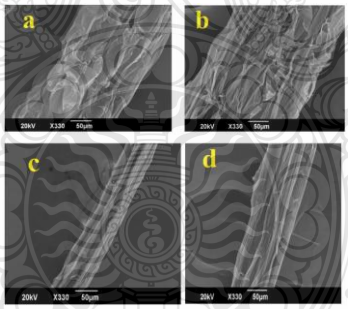

Figure 2.10 SEM images of (a) 5 days aerobic retted fiber (b) 5 days anaerobic retted fiber (c) 5 days aerobic retted fiber after alkali treatment (d) 5 days anaerobic retted fiber after alkali treatment

2.3.2 Chemical composition

The FTIR peak positions can effectively reveal the chemical properties and components of cellulose fibers. Table 2.3 provides a compilation of peak positions and their corresponding meanings.

Table 2.3 FTIR band assignments of cellulose fibers

Wavenumber	Functional group	Molecule	Ref
1730-1735	C=O stretching in unconjugated ketones aldehydes and carboxyl	Xylan, hemicellulose and Pectin	[23, 24]
1595-1606	C=C stretching of the aromatic ring	Lignin	[23, 24]
1508-1514	C=C stretching of the aromatic ring	Lignin	[23, 24]
1458-1463	-C-O-C streching	Lignin	[25]
1362-1375	CH bending	Cellulose	[23, 24, 16]
1314-1317	C–C-H, C-O–H, and CH_2 bending.	Cellulose (crystallised I)	[23, 24, 26]
1269	CO stretching	lignin (guaiacyl) and hemicellulose	[24]
1242-1244	CO stretching	Lignin and hemicellulose	[24]
1201-1204	C-OH and C-CH	Lignin	[23]
1156-1163	COC asym. bridge oxygen stretching	Cellulose	[24]
1101-1105	V(C-O-C)	glycosidic	[23]
1028-1030	associated C-O stretching	cellulose	[23, 27]
896-897	asym. Out of phase ring stretching	Cellulose	[23, 24, 16]

2.3.3 Crystalline structure

In 2012, Yu et al. [16] studied the extraction of NCC from BBF, specifically exploring crystalline properties. The representative X-ray diffraction image of NCC in Figure 2.11 reveals the most prominent peaks at 15.77°, 21.79°, and 33.81°, resembling the crystalline structure of cotton nanocrystalline cellulose, both categorized under cellulose-I. Interestingly, NaOH pretreatment of BBF pulp did not induce any alterations in the cellulose crystalline structure. During hydrolysis, disruption occurred in the amorphous and microcrystalline regions, while crystalline areas remained intact, resulting in highly crystalline samples. The calculated crystallinity index was 71.98%.

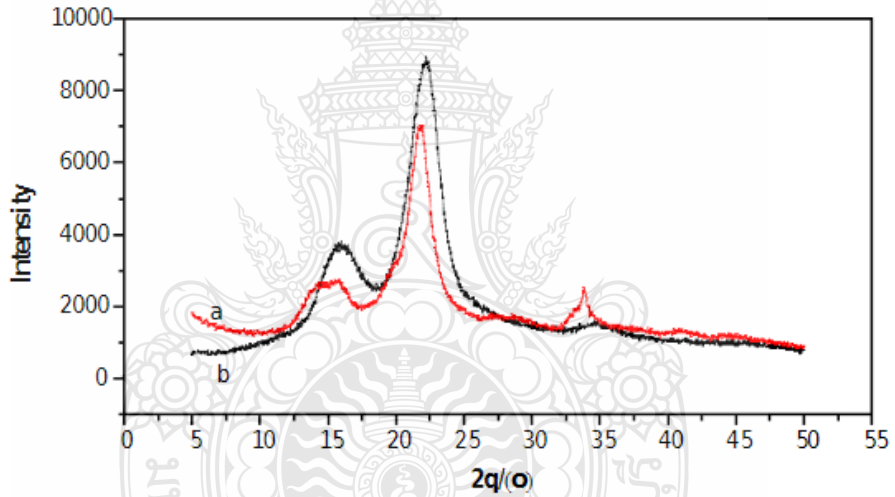

Figure 2.11 X-ray diffraction image of; (a) BBF NCC and (b) cotton NCC

In 2021 Shrestha et al. [28], studied the extraction of NCC from BNNF for antibacterial bio composite reinforcement. The crystalline properties, shown in Figure 2.12, revealed prominent peaks in the NCC diffraction pattern at $2\theta = 15°$, 16°, and 22°, characteristic of native cellulose. BPP exhibited a crystallinity index (CI) of 44.40%, while NCC showed a significantly higher CI of 81.67%. The use of H_2SO_4 selectively penetrated amorphous regions, cleaving glycosidic bonds under hydrolytic conditions.

This process left the crystalline region unaffected, contributing to the enhanced crystallinity of NCC.

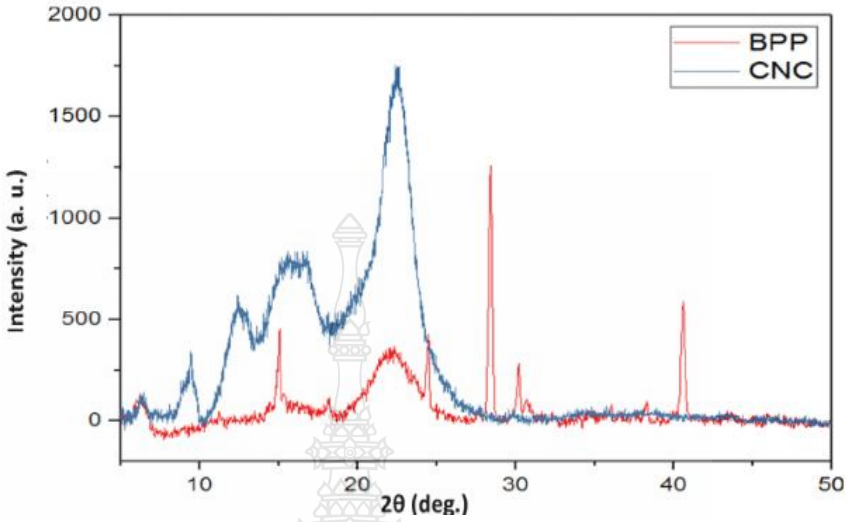

Figure 2.12 X-ray diffraction analysis of crystalline nanocellulose (NCC) and BNNF pseudostem powder (BPP).

In 2017, Asrofi et al. [29], examined the crystalline properties of NCC from WHF at various stages: raw, digester, bleaching, and ultrasonic homogenizing. Figure 2.13 illustrates that the raw fiber presents a flat diffracting pattern with numerous amorphous regions. Conversely, the XRD patterns of digester, bleaching, and ultrasonic homogenized fibers share the same cellulose type I crystal structure with peaks at (2θ = 22.6° and 16°). The consecutive crystallinity indices for raw, digester, bleaching, and ultrasonic homogenized WH fibers were 7%, 68%, 69%, and 73%, respectively. This highlights the effective role of chemical treatment in increasing cellulose fiber crystallinity by removing hemicellulose and lignin contents during processing.

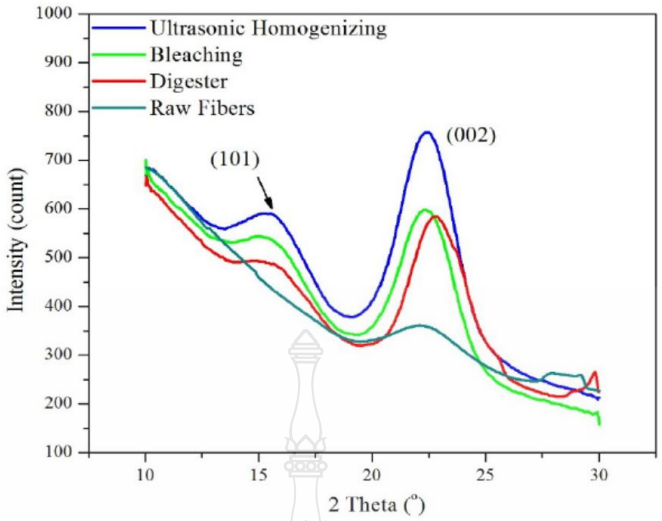

Figure 2.13 XRD pattern of fibers at various stages of treatment

In 2019 Jose M. et al. [30], investigated the unique properties of nonmercerized type-II cellulose, focusing on its crystalline structure. Cellulose materials exhibit rich diversity in crystalline allomorphs (Figure2.14), with types I and II being notable.

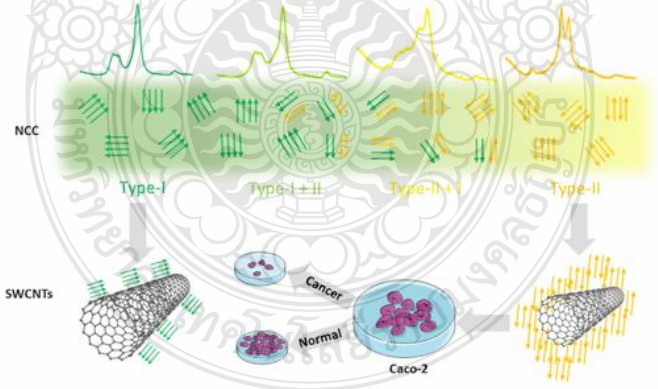

Figure 2.14 Variations in XRD peaks based on cellulose type.

Unlike naturally occurring type I, type II typically requires harsh mercerization conditions. The study introduces a mercerization-free method using acid hydrolysis to produce either type-I or type-II nanocrystalline cellulose (NCC). The

significance lies in the potential to obtain nonmercerized type-II NCC, known for its particularly appealing properties.

In 2023 Phupantrakul et.al. [20], delved into AC from eucalyptus, shedding light on its crystalline structure. (Figure 2.15) XRD patterns reveal the shift from cellulose I to cellulose II during gelatinization and regeneration of semicrystalline eucalyptus paper. Eucalyptus paper exhibits cellulose I peaks at 17.1 and 22.7°, boasting a high crystallinity index (83%). Conversely, AC and ACGO bead patterns display a broad peak at 21.9°, hinting at cellulose II or AC. CI% for AC and ACGO bead can't be calculated due to the complete transformation of semicrystalline cellulose during the gelatinization process.

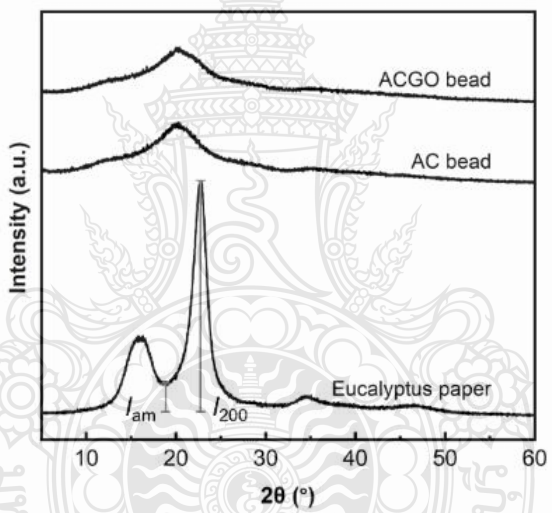

Figure 2.15 XRD patterns for eucalyptus paper, AC and ACGO beads.

2.3.4 Yield

Historically, numerous researchers have dedicated efforts to discover optimal conditions for nanocrystalline cellulose production. However, the yield has consistently remained below 40%, indicating inefficiency for industrial applications. An illustration of parameters and corresponding yield percentages is provided in Table 2.4.

Table 2.4 Literature review of acid hydrolysis method and yield of NCC

Cellulose	Method	% yield	Ref.
Commercial micro cellulose	H_2SO_4 (63.5% w/w) at 50°C for 2 h	30%	[31]
Commercial micro cellulose	H_2SO_4 (64% w/w) at 65°C for 25 min	35%	[32]
Softwood craft pulp	H_2SO_4 (64% w/w) at 45°C for 25 min	32.9	[33]
Water hyacinth	HCl at 60°C for 20 h.	Not reported	[34]
Water hyacinth	5 M of HCl at 50°C for 12 h	Not reported	[13]
Water hyacinth	H_2SO_4 (64 wt%) at 45°C for 30 min	33.69%	[35]
BBF	H_2SO_4 (65 wt%) at 60°C for 12 min	30%	[36]
Banana	H_2SO_4 (concentrated) at 50°C for 30-240 min	Not reported	[15]

2.3.5 Morphology

In 2018, Jose et al. [37], conducted a study on modified NCC for integration with polylactic acid. Regarding morphology, Figure 2.16 presents a representative TEM micrograph of NCC, confirming the successful isolation of NCC. These NCC exhibit a tendency to aggregate after drying, attributed to the absence of surface charge. The measured dimensions of the NCC are 250 nm in length and 35 nm in width.

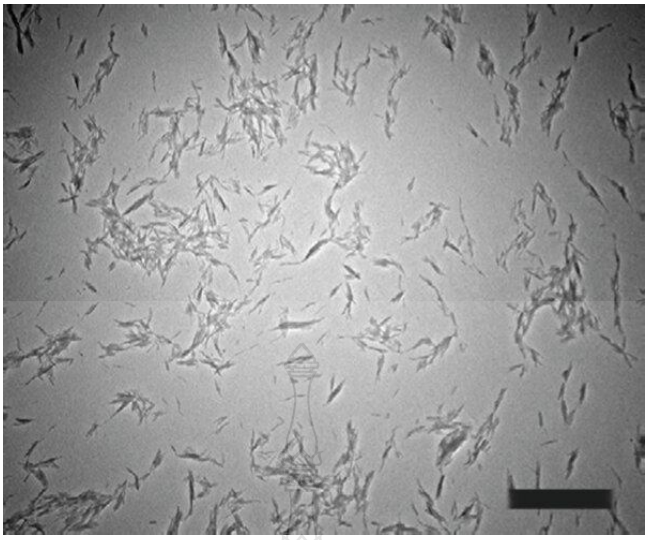

Figure 2.16 TEM image of NCC

In 2020, Lui et.al. [38] investigated the extraction of NCC from rice straw, successfully demonstrating that rice straw can be transformed into NCC. The outcomes, depicted in Figure 2.17, illustrate the geometry of NCC observed through TEM. The extracted NCC from rice straw measured approximately 100 nm in length and 10–15 nm in width.

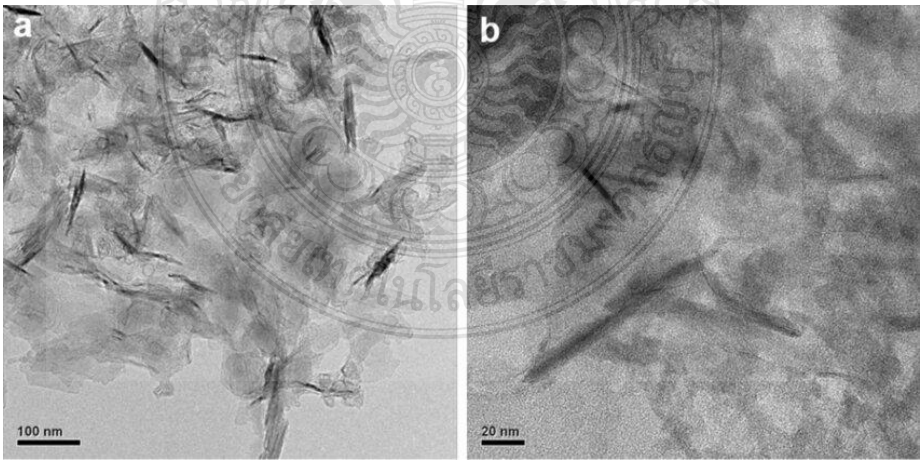

Figure 2.17 TEM image of NCC from rice straw

In 2012 Bernado et.al. [36] conducted a study on the preparation of NCC from BBF. The results, depicted in Figure 2.18, showcase TEM images of negatively stained eucalyptus (Figure 2.18a), sisal (Figure 2.18b), curauá ((Figure 2.18c), and BBF (Figure 2.18d) NCC. Across all cellulose types, the images reveal rodlike nanoparticles and some bundles, potentially influenced by the aggregating effect during drying and/or staining. The NCC length and width were measured from TEM images and averaged for each cellulose source. The average length ranges from 100 to 130 nm, reflecting significant polydispersity. The average nanoparticle width, derived from TEM measurements, varies from 5 to 8 nm, depending on the source.

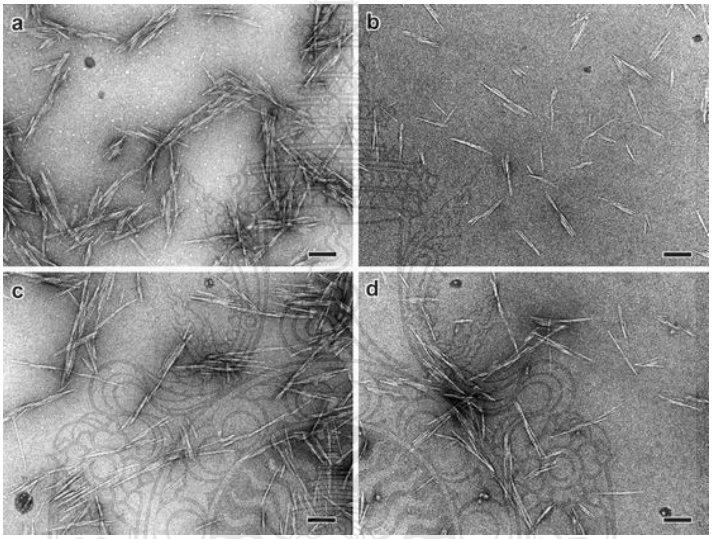

Figure 2.18 TEM image (Scale bars: 100 nm) NCC from; (a) eucalyptus, (b) sisal, (c) curauá, and (d) BBF

CHAPTER 3
RESEARCH METHODOLOGY

The aim of this study is to investigate nanocrystals cellulose (NCC) and amorphous cellulose (AC) derived from bamboo (BBF), banana (BNNF), and water hyacinth (WHF) through H_2SO_4 treatment. The variables under examination include acid concentration, reaction temperature, and hydrolysis time. Morphological analysis, examination of chemical properties, assessment of crystalline structure, and particle size analysis were performed on the NCC and AC. The variables assessed encompassed the percentage of NCC and AC.

3.1 Materials and Chemical

3.1.1 Bamboo sawdust, originating from Prachinburi province, Thailand, were derived from Pimtha co.,ltd in Prachinburi province, Thailand.

3.1.2 Banana stem harvested from local farmers in Pathum-Thani Province

3.1.3 Water hyacinth harvested from river in Pathum-Thani Province

3.1.4 Sulfuric acid (H_2SO_4; ≥ 98.0%, Anapure, New Zealand)

3.1.5 Hydrogen peroxide (H_2O_2; 50% v/v, SOLVAY, Thailand)

3.1.6 Sodium hydroxide (NaOH; 99%, Qrec, New Zealand)

3.2 Experimental

3.2.1 Pretreatment of cellulose fibers

The BBF fiber, BNNF fiber, and WHF underwent boiling in tap water at 90°C for 60 min. Subsequently, the fibers underwent treatment with a 2M NaOH solution at 90°C for 60 min, repeated twice, to purify cellulose by removing constituents such as lignin and hemicellulose. Following the alkali treatment, the fibers were filtered through a No. 18 sieve and washed with distilled water until the alkali was eliminated. A subsequent H_2O_2 bleaching treatment was carried out, using a solution with a 0.05M aqueous NaOH buffer and 10% v/v aqueous H_2O_2, as illustrated in the process flow in Figure 3.1. After the bleaching treatment, the fibers were filtered through a No. 18 sieve and washed with distilled water until reaching a pH of 7.

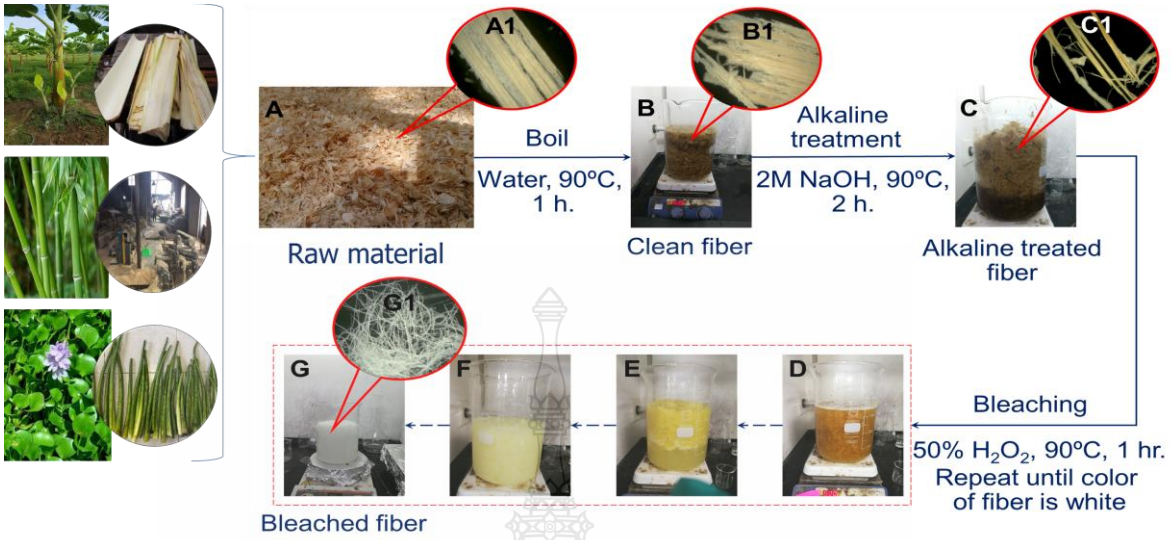

Figure 3.1 Pretreatment process

3.2.2 Preparation of NCC.

The acid hydrolysis method was employed to generate NCC from bleached cellulose obtained from BBF, BNNF, and WHF. A 10 g sample of dried, bleached cellulose was treated with a 50% H_2SO_4 solution 100 ml (with a ratio of 1 g/10 ml) at varying reaction temperatures (50 °C or 60 °C) for different reaction times (15 min, 30 min, 60 min, and 120 min) using a magnetic stirrer. To halt the reaction, 400 ml of deionized (DI) water was added to the mixture, followed by centrifugation at 10,000 rpm and 25°C for 10 min (Frontier PerkinElmer). The flow birefringence of the resulting NCC was determined using a cross-polarized light setup. This process was repeated until the aqueous NCC suspension exhibited flow birefringence, as shown in Figure 3.2b. The NCC suspension was subsequently dialyzed against deionized water, and this step was reiterated until reaching a pH of 7.

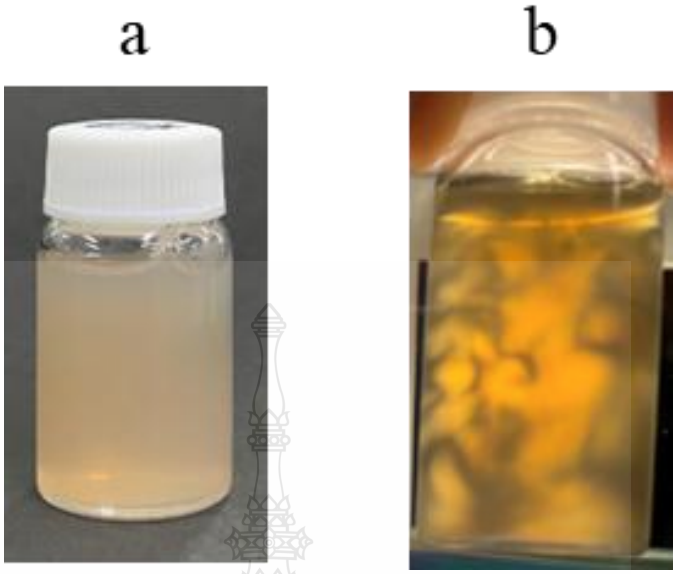

Figure 3.2 Indicator of NCC forming: (a) under normal light, (b) under cross-polarized light setup

3.2.3 preparation of AC

To prepare AC, oven-dried bleached cellulose dissolution using a diluted 60% v/v H_2SO_4 solution. In this process, 1 g of bleached cellulose was treated with 40 ml of H_2SO_4 solution, adding 5 ml increments every 5 min under constant magnetic stirring at 800 rpm, at 0 °C in an ice bath. The procedure concluded when the mixture transformed into a clear gel, as shown in Figure 3.3. To eliminate H_2SO_4, 1500 ml of deionized (DI) water was introduced to the clear mixture and stirred using an overhead stirrer at 1500 rpm before centrifugation at 3500 rpm and 20°C for 3 min. The resulting aqueous amorphous suspension was neutralized by adding 500 ml of DI water and subjecting it to centrifugation at 3500 rpm for 5 min at 20°C. This process was iterated until the pH reached 6, with a note that the initial pH of the DI water was 6.

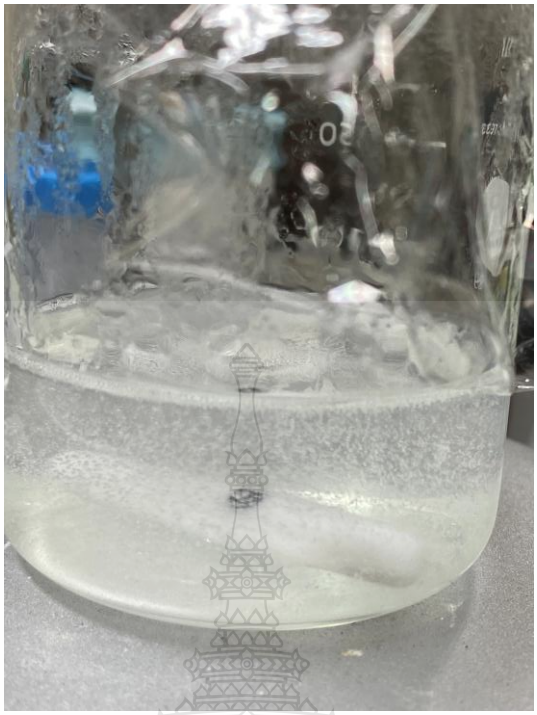

Figure 3.3 Indicator of successful of AC

3.3 Characterization

3.3.1 Yield of NCC and AC

The yield of cellulose (%) obtained was calculated by equation (1) [39].

$$\text{Yield (\%)} = [(W_f)/(W_i)]\text{x}100\% \quad (1)$$

Where W_f is the weight of final cellulose (either NCC or AC) in its dried state, and W_i is the initial weight of the fiber (bleached cellulose).

3.3.2 Fourier transform infrared spectroscopy (FTIR)

The alterations in chemical compositions were investigated across various stages, encompassing raw fiber, alkali fiber, bleached fiber, NCC, and AC. This comprehensive analysis was conducted utilizing a Perkin Elmer FTIR spectrometer. To facilitate precise observations, the samples underwent a drying process, and their respective spectra were meticulously recorded in absorption mode. The spectral readings spanned a range from 4000 to 650 cm^{-1}, and each sample was subjected to 16 scans,

ensuring a thorough and detailed examination of the chemical transformations occurring during the fiber processing stages.

3.3.3 X-ray diffraction

XRD analysis was conducted at the Thailand Institute of Scientific and Technological Research (TISTR) using a copper anti-cathode operating at 40 kV and 40 mA. The scattered intensities were systematically measured across the 2θ angular domain, ranging from 5° to 50°, with a total measurement time of 58 min. Employing a linear detector with an angular aperture of 3°, the diffraction patterns were obtained from power samples uniformly distributed on a neutral quartz glass sample holder. The cellulose crystallinity index was subsequently calculated from the X-ray diffraction patterns, utilizing a predefined equation (2). This meticulous XRD examination provides valuable insights into the structural characteristics and crystalline nature of the samples under investigation [40].

$$\mathrm{CrI}(\%) = \left(\frac{I_{002} - I_{am}}{I_{002}}\right) x100 \qquad (2)$$

Where I_{002} was the intensity of the I_{002} crystalline peak at 22° and I_{am} are the height of the minimum between I_{002} and the I_{101} peaks at 18°.

3.3.4 Scanning electron microscopy (SEM)

A comprehensive examination of sample morphology was utilizing a Scanning Electron Microscope (SEM), using a JEOL model JSM-5410LV, operating at an accelerating voltage of 5 kV. To enhance imaging precision, the dried samples underwent a meticulous coating process involving the deposition of a thin gold layer. A systematic approach was adopted, capturing a minimum of five SEM images from random areas for each individual sample. This methodological protocol ensures a thorough and representative analysis of the samples, providing valuable insights into their surface characteristics and structural features.

3.3.6 Transmission electron microscopy (TEM)

Transmission electron microscopy (TEM), conducted with a Thermo Scientific model Talos, played a pivotal role in elucidating the morphology and dimensions of both NCC and AC extracted from bleached cellulose. The methodology involved depositing a diluted suspension (0.5 wt%) onto the surface of a meticulously prepared clean carbon grid, which was subsequently coated with a thin carbon film to enhance imaging quality. To ensure optimal contrast in TEM, the sample underwent a controlled drying process at ambient temperature (25 °C) before analysis. The TEM examinations were conducted with an accelerating voltage of 80 kV, providing a detailed and high-resolution depiction of the ultrafine structures and characteristics of the NCC and AC samples obtained from the bleached cellulose.

3.3.7 Particle analyzer

The zeta-potential analysis of suspensions containing NCC and AC at a concentration approximately 0.01 wt% was carried out using a Beckman Coulter model Delsa Nano C instrument. This experimental approach involved minimizing the influence of ionic strength by diluting the NCC and AC suspension in an aqueous standard solution with a pH of 7. The zeta-potential measurements provide valuable insights into the surface charge and colloidal stability of the cellulose particles in suspension, offering a nuanced understanding of their electrostatic interactions. Particularly in terms of their potential applications in various industrial and biomedical fields.

CHAPTER 4
RESEARCH RESULT

4.1 Pretreatment

Pretreatment is a crucial initial step in the process of isolating cellulose from natural fibers and converting it into nanocellulose. The main objective of pretreatment is to eliminate non-cellulosic components, such as lignin and hemicellulose, which can hinder subsequent processing. The bleaching process, carried out at 90°C for 120 minutes with continuous mechanical stirring, was repeated six times for BBF, four times for BNNF, and twice for WHF to ensure effective removal of these interfering substances. This step ensures the purification of cellulose and enhances its suitability for subsequent hydrolysis and the production of NCC and AC.

In Figure 4.1a to 4.1c, representations showcase the observable alterations in the color of fibers post-chemical treatment. Figure 4.1a specifically images the discernible color transformation in BBF fibers, while Figure 4.1b captures the analogous change in BNNF fibers, and Figure 4.1c provides a visual record of the color shift in WHF fibers.

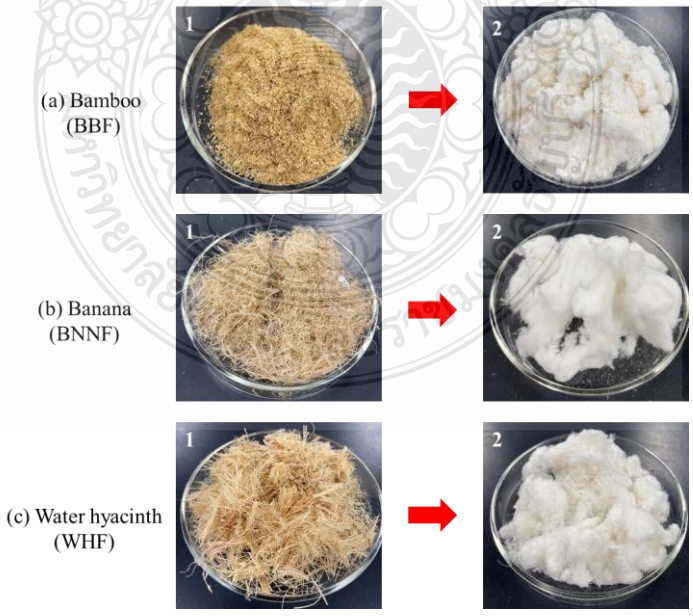

Figure 4.1 Cellulose color changed of: (a) BBF, (b) BNNF, and (c) WHF

Figure 4.1a to 4.1c (left side) of each image reveals the initial brown hue characteristic of the raw fibers, contrasting with Figure 4.2a to 4.2c (right side), where a noticeable transition to a white color is evident. This transformation can be presented to the effective removal of non-cellulosic materials, such as hemicelluloses and lignin, along with the elimination of other impurities like pectin and wax. The chemical treatment, involving processes such as alkalization and bleaching, played a pivotal role in inducing these color changes, underscoring the efficacy of the treatments in purifying, and modifying the fiber composition.

4.2 Effect of pretreatment of cellulose fibers

The microstructure of cellulose fibers plays a significant role in determining their properties and behavior in further processing, especially to produce NCC and AC. Understanding the structural changes that occur during pretreatment is essential to optimize the process and improve the quality of the resulting nanocellulose.

Figures 4.2a to 4.2c provide detailed insights into the microstructural changes observed in BBF, BNNF, and WHF fibers, respectively. The microstructural analysis reveals distinctive transformations in the fibers, particularly evident in the comparison between the Figures 4.2a to 4.2c (left side) representing raw fibers and the Figures 4.2a to 4.2c (right side) illustrating bleached fibers.

In Figures 4.2a to 4.2c (left side), the raw fibers exhibit a bundled arrangement, characterized by thick and rough fibers. As the process progresses to Figures 4.2a to 4.2c (right side), depicting bleached fibers, a discernible refinement is apparent. The fibers become not only thinner but also assume a microfiber configuration, indicative of the profound impact of the bleaching treatment.

This microstructural transformation is directly linked to the removal of non-cellulosic components and impurities, such as pectin and wax, which act as protective layers surrounding cellulose fibers. The outcome is a smoother and more delicate fiber structure, underscoring the efficacy of the bleaching process in enhancing the overall microstructure of the fibers. These micrograph representations serve as valuable visual documentation of the transformative effects of bleaching on the microstructural features

of BBF, BNNF, and WHF fibers, offering deeper insights into the structural modifications induced by the chemical treatments.

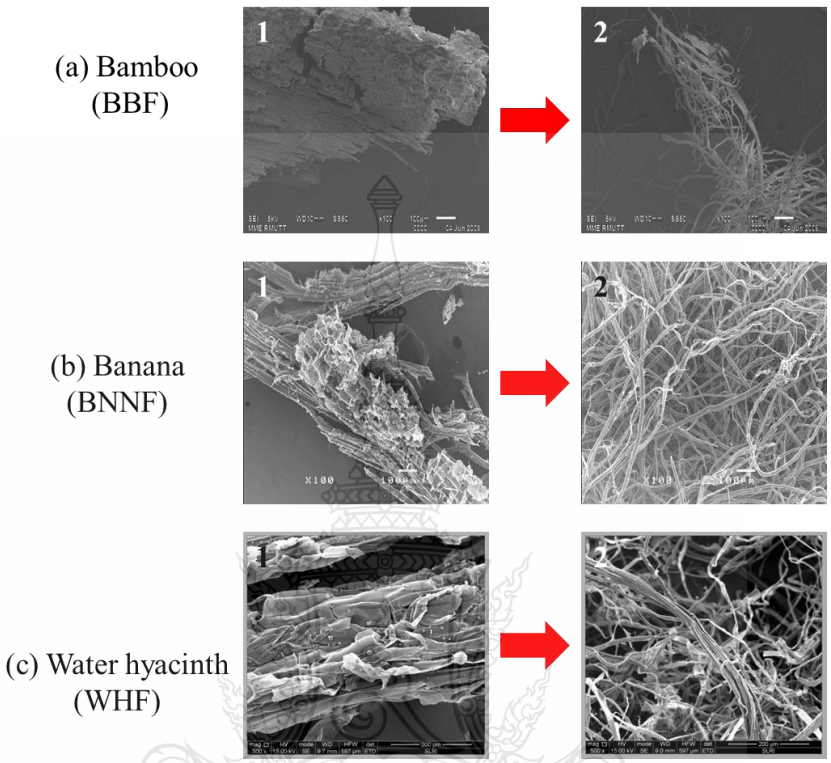

Figure 4.2 Microstructure of: (a) BBF, (b) BNNF, and (c) WHF

4.3 Effect of pretreatment to chemical structure of cellulose fibers

Figures 4.3a and 4.3b present an in-depth analysis of the FTIR spectra, offering a comparative examination between BBF raw fibers and BBF bleached fibers (following the sixth bleaching cycle). In Figure 4.3a, distinctive peaks at 1725 cm^{-1}, 1602 cm^{-1}, 1512 cm^{-1}, 1453 cm^{-1}, and 1262 cm^{-1} signify characteristic impurities, primarily associated with lignin and hemicellulose. Notably, these impurity-related peaks are conspicuously absent in Figure 4.3b, demonstrating the transformative impact of alkalization and subsequent bleaching.

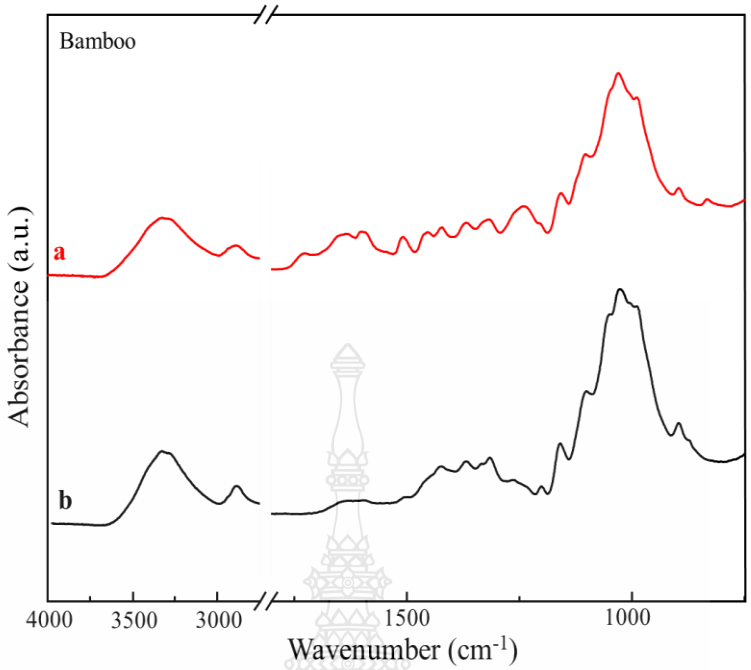

Figure 4.3 FTIR spectra of BBF: (a) raw fibers and (b) bleached fiber

Figures 4.4a and 4.4b respectively, show the FTIR spectra, facilitating a comparative analysis between BNNF raw fibers and BNNF bleached fibers (following the fourth bleaching cycle). In Figure 4.4a, discernible peaks at 1722 cm^{-1}, 1604 cm^{-1}, 1452 cm^{-1}, and 1260 cm^{-1} highlight characteristic impurities, primarily associated with lignin and hemicellulose. The absence of these impurity-related peaks in Figure 4.4b stands out prominently, underscoring the transformative efficacy of both alkalization and subsequent bleaching processes.

Figures 4.5a and 4.5b respectively, depict the FTIR spectra, show comparative analysis between WHF raw fibers and WHF bleached fibers (after the second bleaching cycle). In Figure 4.5a, specific peaks at 1731 cm^{-1} and 1242 cm^{-1} stand out, indicating characteristic features associated with carbonyl stretching in hemicellulose and CO stretching in lignin and hemicellulose, respectively. Notably, these distinctive peaks vanish in Figure 4.5b, following the alkalization and bleaching processes, underscoring their effectiveness in removing lignin and hemicellulose.

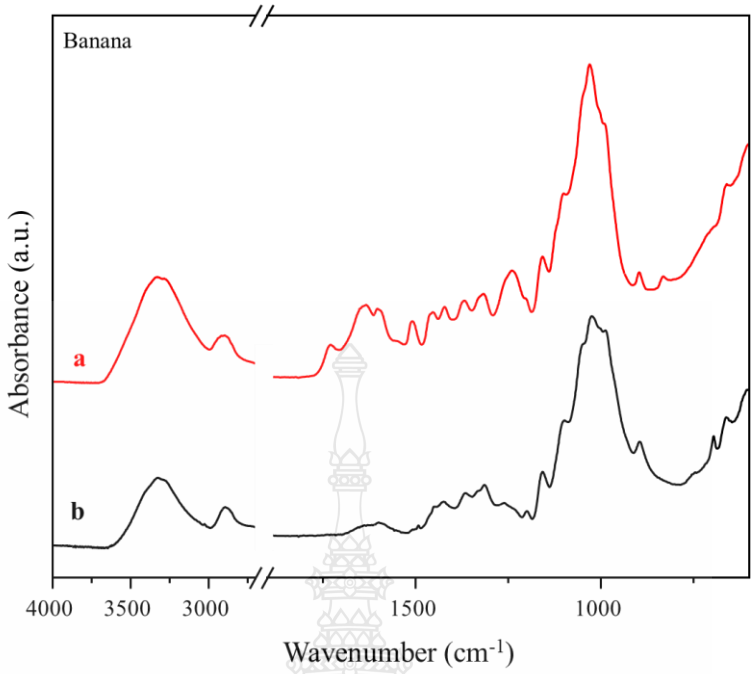

Figure 4.4 FTIR spectra of BNNF: (a) raw fibers and (b) bleached fiber

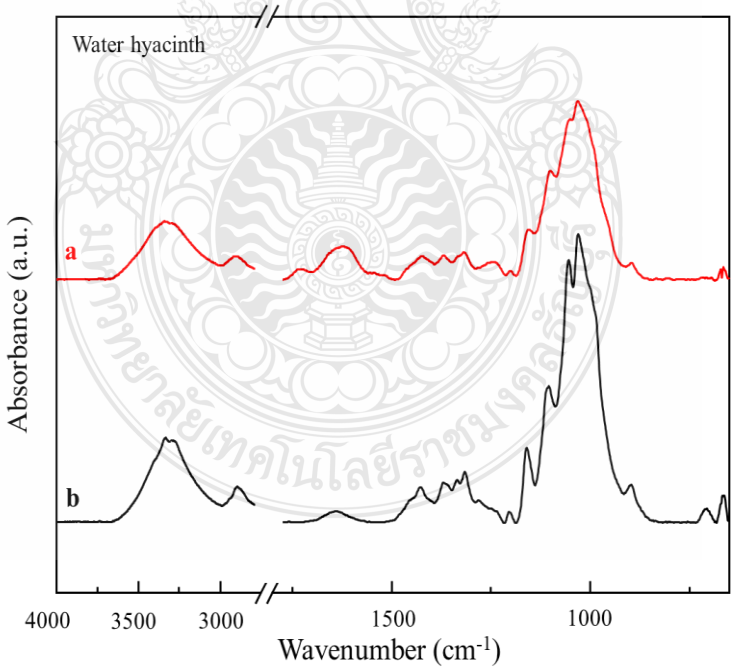

Figure 4.5 FTIR spectra of WHF: (a) raw fibers and (b) bleached fiber.

The disappearance of impurity-related peaks presented the efficacy of alkalization and bleaching processes in effectively eliminating lignin and hemicellulose from the cellulose fibers. The FTIR spectra serves as a powerful analytical tool, enabling a nuanced understanding of the chemical composition alterations induced by the treatment procedures. This comprehensive examination reaffirms the successful removal of impurities, signifying a crucial step in enhancing the purity and compositional integrity of the cellulose fibers.

4.4 Effects of acid treatment conditions on yield of cellulose fibers

After the successful completion of the pretreatment process, which involved the removal of lignin, hemicellulose, and other non-cellulosic components, the cellulose fibers from BBF, BNNF, and WHF were subjected to acid hydrolysis. Acid treatment is a critical step for breaking down the cellulose fibers to produce NCC and AC. The conditions of acid hydrolysis, such as temperature, duration, and acid concentration, significantly affect the yield and characteristics of the resulting cellulose products. Optimizing these conditions is essential for maximizing the yield of nanocellulose while maintaining its desired properties. This section explores the impact of varying acid treatment conditions on the cellulose yield from the pretreated fibers, focusing on how different temperatures and hydrolysis times influence the production of NCC and AC.

4.4.1 Effect of acid hydrolysis of BBF

Figures 4.6 to 4.8 delve into the nuanced effects of variable reaction time (15, 30, 60, and 120 min) and reaction temperature (40 °C, 50 °C, and 60 °C) on the color transformation of BBF-NCC. In Figure 4.6, the conditions leading to the successful production of BBF-NCC are spotlighted, with a reaction temperature of 40 ºC. The color of the solution transitions from white to a subtle light yellow, exhibiting a distinctive change with increasing reaction time (from 30 min to 120 min). In Figure 4.7 and Figure 4.8, wherein the reaction temperature is set at 50 ºC and 60 ºC, respectively, the formation of BBF-NCC is evident across varying reaction times (15 min, 30 min, 45 min, and 60 min). Notably, the color of the solution undergoes a continuum of changes from white to yellow and eventually dark yellow. This visual transformation can be attributed to the

hydrolytic action of H_2SO_4, destroying parts of the amorphous part of cellulose and showing conversion into glucose with prolonged reaction times.

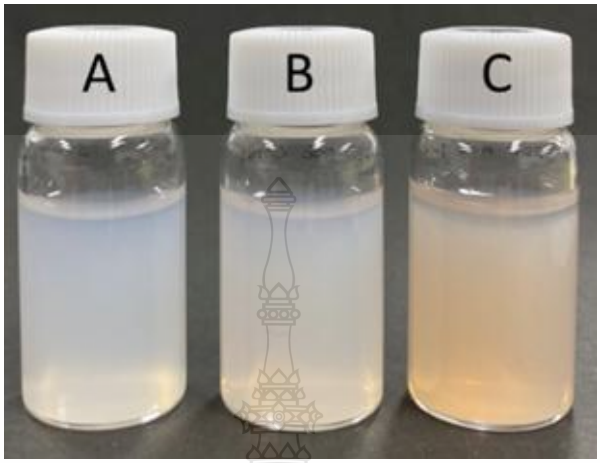

Figure 4.6 Color of BBF-NCC suspension, given the hydrolysis temperatures of 40 °C: (A) 30 min, (B) 60 min, (C) 120 min

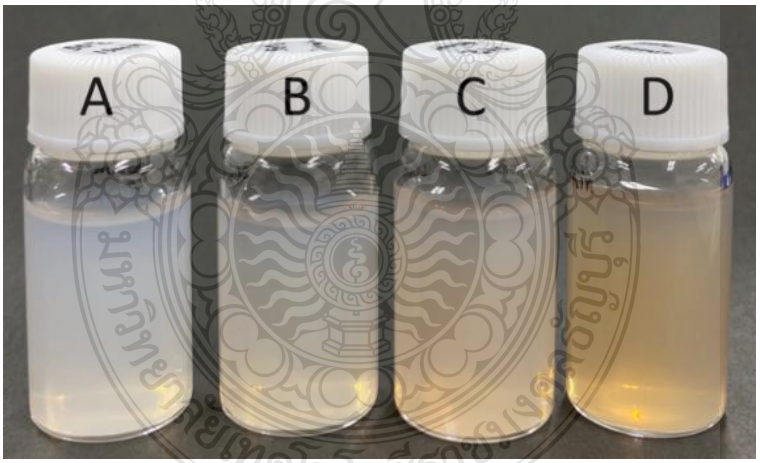

Figure 4.7 Color of BBF-NCC suspension, given the hydrolysis temperatures of 50 °C: (A) 15 min, (B) 30 min, (C) 60 min, (D) 120 min.

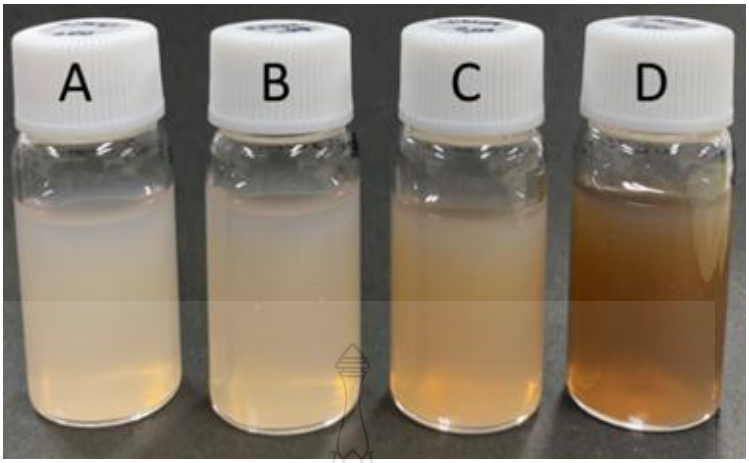

Figure 4.8 Color of BBF-NCC suspension, given the hydrolysis temperatures of 60 °C: (A) 15 min, (B) 30 min, (C) 60 min, (D) 120 min

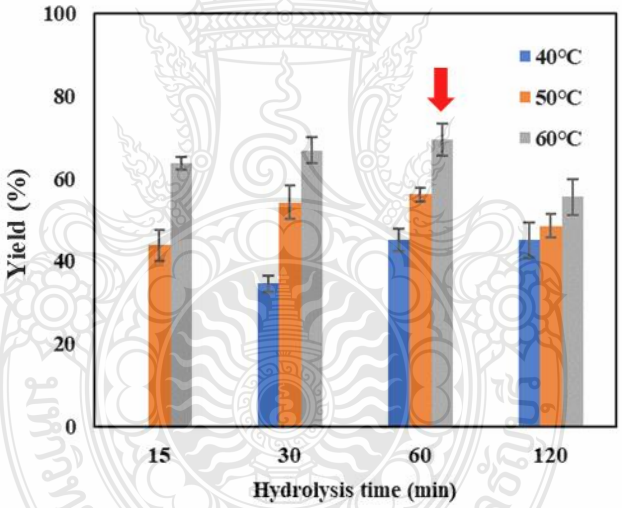

Figure 4.9 The yield of BBF-NCC under variable hydrolysis times given the hydrolysis temperatures of 40, 50 and 60 °C

In Figures 4.9, the BBF-NCC yields are systematically presented under diverse combinations of reaction temperatures and times. The highest BBF-NCC yield, reaching 69.46%, is achieved under specific hydrolysis conditions involving 50%v/v H_2SO_4, a reaction temperature of 60 °C, and a reaction time of 60 min. These

comprehensive yield analyses provide valuable insights into the intricate interplay between reaction conditions and the resulting characteristics of BBF-NCC, contributing to a deeper understanding of the optimal parameters for their efficient production.

4.4.2 Effect of acid hydrolysis of BNNF

Figures 4.10 to 4.12 show the effects of variable reaction time (15, 30, 60, and 120 min) and reaction temperature (40 °C, 50 °C, and 60 °C) on the color transformation of BNNF-NCC. In Figure 4.10, the conditions leading to the successful production of BNNF-NCC are spotlighted, with a reaction temperature of 40 °C. The color of the solution transitions from light yellow to yellow, exhibiting a distinctive change with increasing reaction time (from 30 min to 120 min). In Figure 4.11 and Figure 4.12, wherein the reaction temperature is set at 50 °C and 60 °C, respectively, the formation of BNNF-NCC is evident across varying reaction times (15 min, 30 min, 45 min, and 60 min). Notably, the color of the solution undergoes a continuum of changes from yellow to dark yellow. This visual transformation can be attributed to the hydrolytic action of H_2SO_4, destroying parts of the amorphous part of cellulose and showing conversion into glucose with prolonged reaction times.

Figure 4.10 Color of BNNF-NCC suspension, given the hydrolysis temperatures of 40 °C: (A) 30 min, (B) 60 min, (C) 120 min

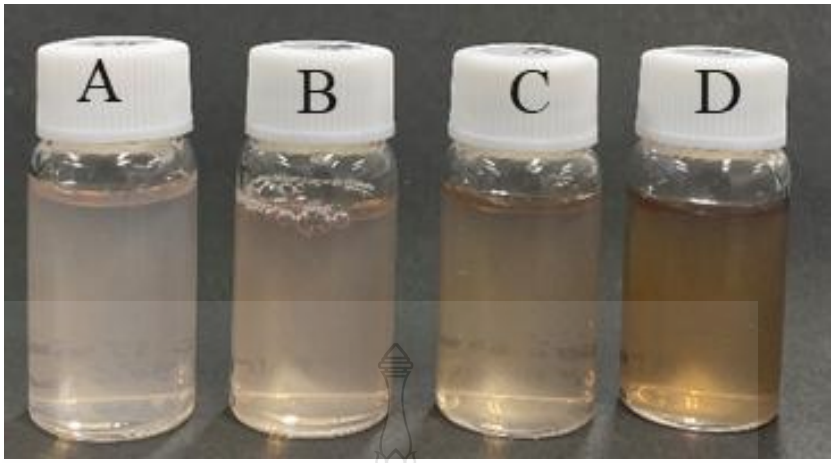

Figure 4.11 Color of BNNF-NCC suspension, given the hydrolysis temperatures of 40 °C: (A) 30 min, (B) 60 min, (C) 120 min

Figure 4.12 Color of BNNF-NCC suspension, given the hydrolysis temperatures of 40 °C: (A) 30 min, (B) 60 min, (C) 120 min.

In Figure 4.13, the BNNF-NCC yields are systematically presented under diverse combinations of reaction temperatures and times. The highest BNNF-NCC yield, reaching 68.44%, is achieved under specific hydrolysis conditions involving 50%v/v H_2SO_4, a reaction temperature of 60 °C, and a reaction time of 15 min. These comprehensive yield analyses provide valuable insights into the intricate interplay

between reaction conditions and the resulting characteristics of BNNF-NCC, contributing to a deeper understanding of the optimal parameters for their efficient production.

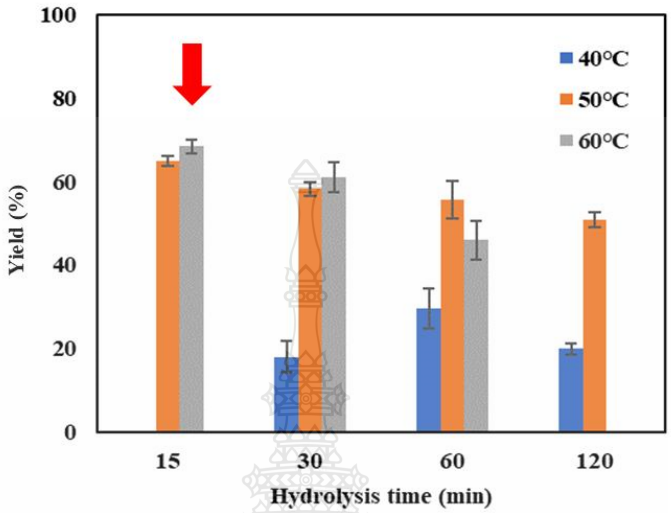

Figure 4.13 The yield of BNNF-NCC under variable hydrolysis times given the hydrolysis temperatures of 40, 50 and 60°C

4.4.3 Effect of acid hydrolysis of WHF

Figure 4.14 shows a comprehensive visual analysis, contrasting the color variations in WHF-NCC subjected to different hydrolysis times (15, 30, 60, and 120 min) at hydrolysis temperatures of 50 and 60°C. At 50°C, the color of WHF-NCC is distinctly observed, transitioning from white to a subtle light yellow across the range of hydrolysis times, spanning from 15 to 120 min. Meanwhile, in Figure 4.15, at a hydrolysis temperature of 60°C, the color of WHF-NCC shows a transformation from white to light brown, correlating with the extended hydrolysis times from 15 to 120 min. It's noteworthy that the acid-hydrolyzed WHF-NCC manifests itself as a colloidal aqueous suspension, signifying the dispersed nature of the NCC in the solution. This in-depth comparison elucidates the impact of both hydrolysis time and temperature on the visual characteristics of WHF-NCC, offering valuable insights into the optimal conditions for the hydrolysis process and subsequent colloidal suspension.

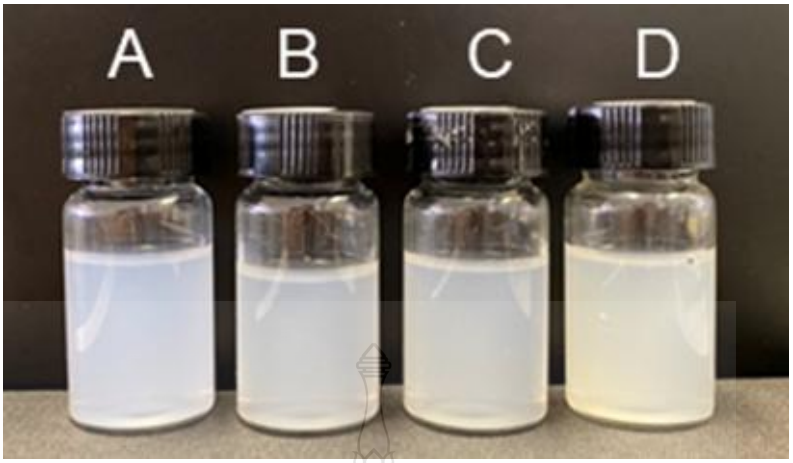

Figure 4.14 Color of WHF-NCC suspension, given the hydrolysis temperatures of 40 °C (A) 30 min, (B) 60 min, (C) 120 min

Figure 4.15 Color of WHF-NCC suspension, given the hydrolysis temperatures of 40 °C: (A) 30 min, (B) 60 min, (C) 120 min.

In Figure 4.16, presented, illustrating the yield variations of WHF-NCC (%), under variable hydrolysis times, considering hydrolysis temperatures of 50 and 60 °C. The results illuminate a discernible positive correlation between the yield of WHF-NCC and both hydrolysis temperature and time. At 50 °C, the impact of hydrolysis time on the WHF-NCC yield appears relatively subdued in comparison to the more pronounced effect observed at 60°C. Particularly is the trend at 60 °C, where the WHF-

NCC yield exhibits a consistent increase with the extension of hydrolysis time, albeit registering a decrease after the 60 min mark. This behavior the intricate between temperature and time in the yield of WHF-NCC. The highest recorded WHF-NCC yield, reaching 85.3%, is achieved under the conditions of 60 °C and 60 min hydrolysis time.

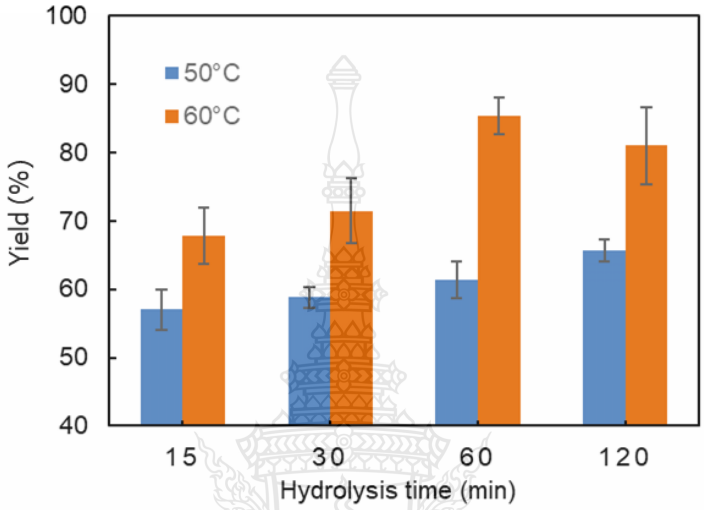

Figure 4.16 The yield of WHF-NCC under variable hydrolysis times given the hydrolysis temperatures of 40, 50 and 60°C

4.4.4 Effect of acid dissolution of BBF, BNNF, and WHF

In this work determining the optimal conditions for acid dissolution to produce AC, a comprehensive experimental approach was employed. Acid concentration was fixed at 60%, while temperature and reaction time were systematically varied within the range of 0 to 50 min, with the reaction temperature carefully controlled at 0 °C and maintained in an ice bath. The experimental findings revealed a critical aspect of the acid dissolution process.

In the experimental procedure, a drop-wise addition of acid solution was carried out over time the condition same as all of the cellulose sources of BBF, BNNF, and WHF. A pivotal observation emerged when all cellulose samples exhibited complete gel formation, signifying the thorough dissolution of the acid in the cellulose chains. This gel formation was consistently achieved at 40 min with an acid solution volume of 40ml.

It is imperative to note that extending the dissolution time beyond this threshold led to the deterioration of cellulose chains, resulting in the degradation to glucose. This intricate balance is crucial in maintaining the effectiveness of yielding AC aqueous suspension.

Figure 4.17 visually captures a show, depicting a cloudy and white-colored solution. The corresponding yields of BBF-AC, BNNF-AC, and WHF-AC were determined to be 65.1%, 62.2%, and 71.6%, respectively.

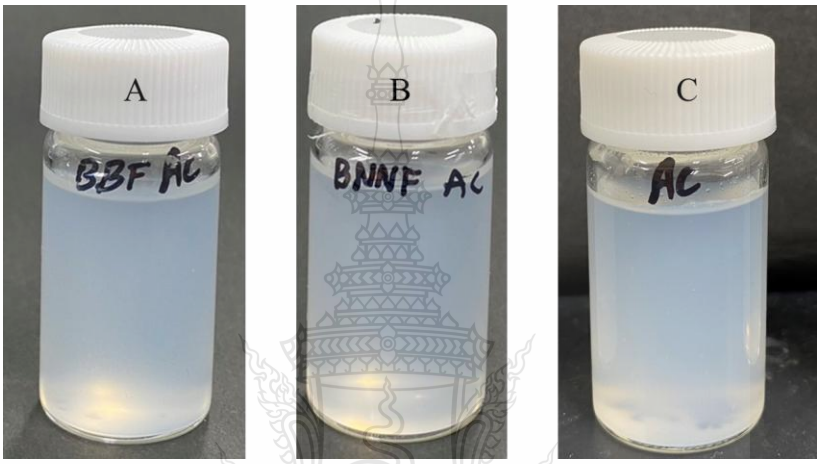

Figure 4.17 AC suspension of: (A) BBF, (B) BNNF and (C) WHF

4.5 XRD crystalline structure of cellulose fibers

Following the successful identification of the optimum acid hydrolysis conditions for each fiber type BBF, BNNF, and WHF. The cellulose samples were further characterized to evaluate their crystalline structure. Understanding the crystalline and amorphous regions of cellulose is essential for distinguishing between NCC and AC, as these characteristics directly influence the mechanical properties and potential applications of the material. To assess the crystallinity of the cellulose fibers, X-ray Diffraction (XRD) analysis was employed. XRD provides valuable insights into the degree of crystallinity by identifying the arrangement of cellulose molecules within the fiber structure. This section presents the results of XRD analysis, highlighting the differences in crystallinity between NCC and AC produced under the optimized conditions.

4.5.1 Crystalline structure of BBF fibers

Figures 4.18A and B show the XRD spectra for BBF-NCC and BBF-AC. The XRD patterns provide the structural characteristics of these cellulose derivatives. In Figure 4.18A, the XRD spectrum of BBF-NCC reveals the presence of two dominant crystalline peaks, I_{002} and I_{101}, at approximately 22.0° and 18°, respectively. The positioning of the peaks at 22° and 18° was determined by crystalline structure associated with cellulose type I.

Figure 4.18B, the XRD spectrum of BBF-AC. The I_{002} peak of BBF-AC experiences a shift to a lower 2θ value, approximately 20°, while the I_{101} peak demonstrates a parallel shift to 16°. These shifts are indicative of the acid-induced dissolution of the crystalline domain in bleached fibers. The emergence of new peaks (I_{002} and I_{101}) signifies a structural transition from cellulose type I to cellulose type II. Cellulose type II, typically associated with man-made cellulose, indicates the destruction of the original cellulose structure (type I) and its regeneration into a new crystalline form (type II).

The determination of crystallinity index for BBF-NCC and BBF-AC was carried out by analyzing the dominant peak (I_{002}) at 22°, whereas the crystallinity index for BBF-AC was based on the I_{002} peak at 20°. The resulting crystallinity index was determined to be 89.5% for BBF-NCC and 35.4% for BBF-AC. The notably higher crystallinity index observed in BBF-NCC can be attributed to the acid hydrolysis process effectively eliminating amorphous regions, leaving behind a more crystalline structure. This enhanced crystallinity is indicative of the successful removal of disordered cellulose components, resulting in a NCC material with a pronounced structural regularity.

Conversely, BBF-AC exhibits a lower crystallinity index, primarily owing to the dissolution of the crystalline domain during acid treatment. The subsequent regeneration of the crystalline structure leads to a less ordered and more amorphous cellulose form. The marked difference in crystallinity indices between BBF-NCC and BBF-AC the transformative impact of acid-induced processes on the structural characteristics of these cellulose derivatives.

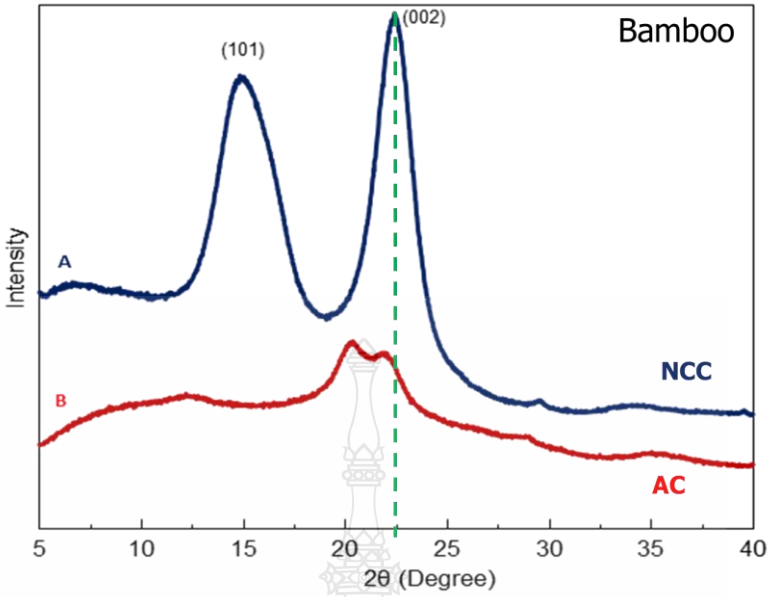

Figure 4.18 XRD pattern of: (A) BBF-NCC and (B) BBF-AC

4.5.2 Crystalline structure of BNNF fibers

Figures 4.19A and B depict the XRD spectra of BNNF-NCC and BNNF-AC. In Figure 4.19A, dominant crystalline peaks at approximately 22.3° and 18.2° confirm BNNF-NCC indicated with cellulose type I. Figure 4.19B shows shifts in the I_{002} peak of BNNF-AC to around 20.2° and I_{101} to 16.3°, indicating acid-induced crystalline domain dissolution and regeneration, transforming cellulose type I to type II.

Crystallinity index for BNNF-NCC and BNNF-AC, calculated based on the dominant peak (I_{002}) at 22.3° and 20.1°, respectively, were 82.3% and 28.4%. BNNF-NCC higher index suggests efficient amorphous region removal, while BNNF-AC's lower index reflects the dissolution and regeneration of a less ordered crystalline structure.

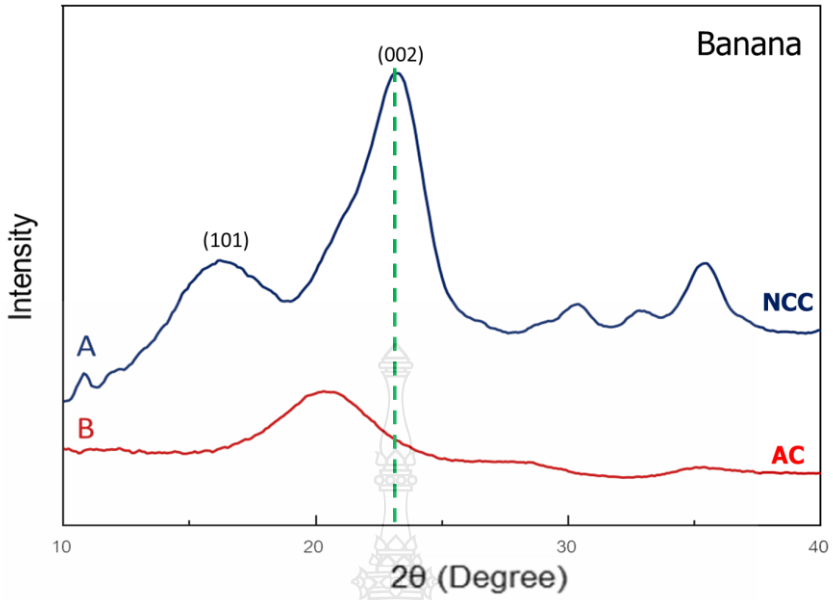

Figure 4.19 XRD pattern of: (A) BNNF-NCC and (B) BNNF-AC

4.5.3 Crystalline structure of WHF fibers

Figures 4.20A and B depict the XRD spectra of WHF-NCC and WHF-AC. In Figure 4.20A, dominant crystalline peaks at approximately 22.1° and 18.0° confirm WHF-NCC indicated with cellulose type I. Figure 4.20B shows shifts in the I_{002} peak of BNNF-AC to around 20.4° and I_{101} to 16.1°, indicating acid-induced crystalline domain dissolution and regeneration, transforming cellulose type I to type II.

Crystallinity index for WHF-NCC and WHF-AC, calculated based on the dominant peak (I_{002}) at 22.1° and 20.4°, respectively, were 87.67% and 26.2%. WHF-NCC higher index suggests efficient amorphous region removal, while WHF-AC lower index reflects the dissolution and regeneration of a less ordered crystalline structure.

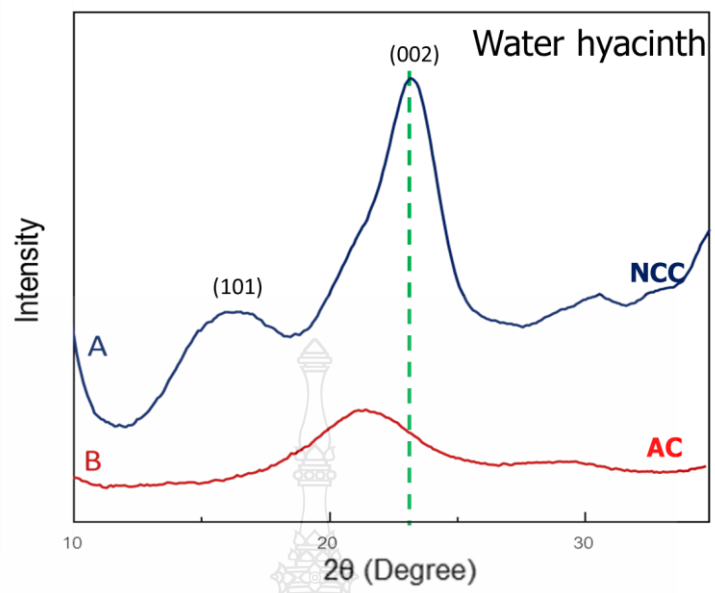

Figure 4.20 XRD pattern of: (A) WHF-NCC and (B) WHF-AC

4.6 TEM morphology

Following the optimization of acid hydrolysis conditions, Transmission Electron Microscopy (TEM) was used to examine the morphology of the Nanocrystalline Cellulose (NCC) produced from Bamboo Fiber (BBF), Banana Fiber (BNNF), and Water Hyacinth Fiber (WHF). TEM provided insights into the particle size, shape, and structural characteristics of the NCC, which are critical for its application in nanocomposites and other materials.

Figure 4.21 A-C TEM images, focusing on BBF-NCC, BNNF-NCC, and WHF-NCC, respectively. The NCC derived from all plant sources, including BBF, BNNF, and WHF, exhibit a distinctive whisker shape morphology. This characteristic shape arises from the acid hydrolysis process, which effectively destroyed the amorphous domains of cellulosic microfibrils (bleached fibers), while preserving the crystalline domains.

The dimensions and length ratios of the NCC were shown (Figure 4.21A-C) for all samples. Notably, the diameters of the NCC fell within the range of 4–20 nm, the lengths varied between 50–500 nm. The size, length, and structural characteristics of the NCC produced from BBF, BNNF, and WHF. The whisker-shaped morphology and well-defined dimensions highlight the success of acid hydrolysis in selectively breaking down

amorphous regions, resulting in NCC with distinct crystalline features. Figure 4.21 A-C, therefore, serves as a comprehensive visual representation of the NCC morphology derived from different plant sources, enhancing our understanding of their structural nuances.

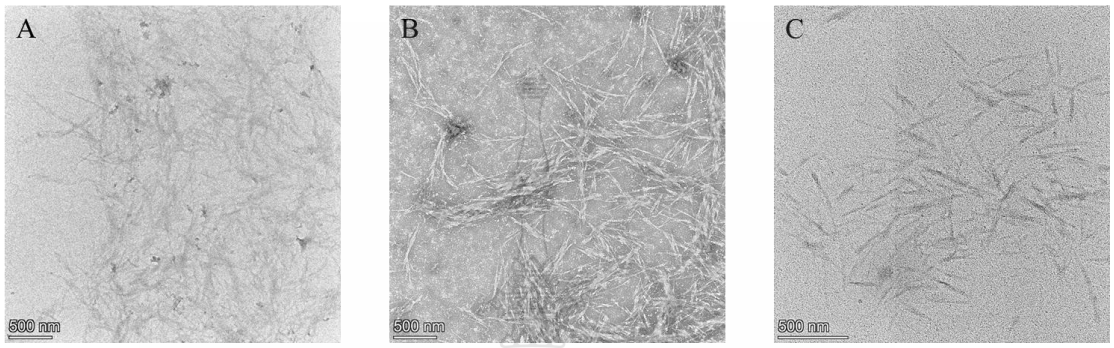

Figure 4.21 TEM image of: (A) BBF-NCC, (B) BNNF-NCC and (C) WHF-NCC

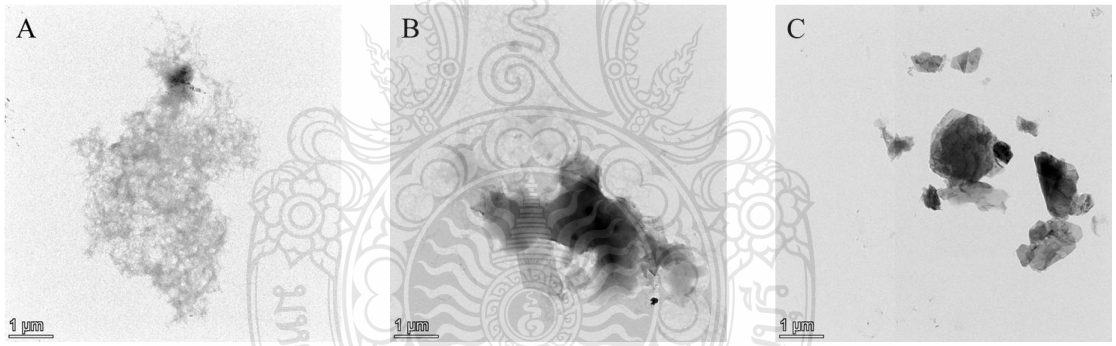

Figure 4.22 TEM image of: (A) BBF-AC, (B) BNNF-AC and (C) WHF-AC

In Figure 4.22A–C, a comprehensive exploration of the TEM images is presented, focusing on AC derived from BBF-AC, BNNF-AC and WHF-AC, respectively. The AC originating from all plant sources demonstrates a distinctive clustering phenomenon, showcasing a diverse array of cluster sizes. This clustering effect is a result of the sulfuric acid's thorough dissolution of the crystalline domains present in the bleached fibers. The acid effectively dissolves the existing crystalline structures, the

way for the regeneration of new crystalline domains characterized by a random particle size distribution.

4.7 The zeta potential

After optimizing the production of NCC from BBF, BNNF, and WHF, zeta potential measurements were conducted to assess the colloidal stability of the NCC suspensions. Zeta potential is a key indicator of surface charge and stability in dispersion systems, with higher absolute values suggesting better stability.

The zeta potential, as detailed in Table 4.1, offers the colloidal stability of NCC and AC derived from various plant sources, including BBF, BNNF, and WHF. The zeta potential measurements for BBF-NCC, BNNF-NCC, and WHF-NCC were recorded as -30.93 mV, -43.21 mV, and -33.24 mV, respectively. The zeta potential for BBF-AC, BNNF-AC, and WHF-AC were noted as -19.73 mV, -18.46 mV, and -17.25 mV, respectively.

Table 4.1 Zeta potential of NCC and AC from plant

Cellulose	Zeta potential (mV)
BBF-NCC	-30.93
BNNF-NCC	-33.21
WHF-NCC	-43.24
BBF-AC	-19.73
BNNF-AC	-18.46
WHF-AC	-17.25

A zeta potential below -30 mV or above 30 mV is indicative of high colloidal stability. In this research, the consistently negative zeta potential values signify enhanced colloidal stability attributed to the integration of charged sulfate ester groups induced by H_2SO_4 onto the surfaces of both NCC and AC. The negative zeta potential plays a crucial role in preventing the aggregation of particles, thus ensuring a stable colloidal suspension. This analysis contributes to a comprehensive understanding of the electrostatic

interactions governing the stability of NCC and AC, elucidating the successful modification achieved through the sulfation process.

CHAPTER 5
CONCLUSION AND RECOMMENDATIONS

This experimental study delved into the effects of various acid treatment methods on the physicochemical attributes of nanocellulose derived from three plant sources (BBF, BNNF, and WHF). The acid treatment methods encompassed sulfuric acid hydrolysis for NCC and sulfuric acid dissolution for AC, focusing on the crystalline structure, morphology, and colloidal stability of BBF, BNNF, and WHF nanocellulose.

The optimized acid hydrolysis processes resulted in high yields of cellulose for all three fiber types. The highest NCC yield was obtained from WHF at 85.3% with 50%v/v H_2SO_4, 60 °C, and 60 min, followed by BBF at 69.46% with 50%v/v H_2SO_4, 60 °C, and 60 min., and BNNF at 68.44% with 50%v/v H_2SO_4, 60 °C, and 15 min.

The optimized acid dissolution processes resulted in high yields of cellulose for all three fiber types. The highest AC yield was obtained from WHF at 71.6%, followed by BBF at 65.1%, and BNNF at 62.2% with 60%v/v H_2SO_4, 0 °C, and 40 min.

The results revealed that NCC exhibited notably higher crystallinity indices: 89.5% for BBF, 82.3% for BNNF, and 87.67% for WHF, in contrast to 35.4%, 28.4%, and 26.2% for BBF-AC, BNNF-AC, and WHF-AC, respectively. This heightened crystallinity of NCC was attributed to the efficient removal of amorphous regions through acid hydrolysis, while the lower crystallinity of BBF-AC resulted from the disruption of crystalline regions during acid dissolution.

TEM analysis demonstrated that NCC featured a whisker shape with diameters ranging from 4 to 20 nm and lengths from 5 to 500 nm, whereas AC aggregated into clusters of varying sizes. Furthermore, NCC exhibited superior colloidal stability compared to AC, evident in zeta potentials of −30.93 mV, -33.21mV, and -43.24 mV for BBF-NCC, BNNF-NCC, and WHF-NCC, respectively, in contrast to −19.73 mV, -18.46 mV, and -17.25mV for BBF-AC. Acid treatment notably enhanced the zeta potentials of BBF-NCC and BBF-AC, BNNF-AC, and WHF-AC.

Importantly, both NCC and AC demonstrate potential applications as reinforcing agents in bio composites or as carriers in various industrial applications. Notably, this research marks the first instance of converting bamboo sawdust, water

hyacinth from river and waste management for banana stem post-harvest. A byproduct from agriculture waste, into cellulose nanofibers a sustainable and economically viable solution to waste from agriculture.

List of Bibliography

[1] X. Y. Du, Q. Li, G. Wu, and S. Chen, “Multifunctional micro/nanoscale fibers based on microfluidic spinning technology,” *Advanced Materials,* vol. 31, no. 52, pp. 1903733, 2019.

[2] S. Srivaro, “Potential of three sympodial bamboo species naturally growing in Thailand for structural application,” *European journal of wood and wood products,* vol. 76, no. 2, pp. 643-653, 2018.

[3] P. Anupunt, “Banana in Thailand,” *Advancing banana and plantain R&D in Asia and the Pacific-Vol. 11*, pp. 149, 2002.

[4] J. Mahujchariyawong, and S. Ikeda, “Modelling of environmental phytoremediation in eutrophic river—the case of water hyacinth harvest in Tha-chin River, Thailand,” *Ecological modelling,* vol. 142, no. 1-2, pp. 121-134, 2001.

[5] Z. Li, D. Wang, P. Sui, P. Long, L. Yan, X. Wang, P. Yan, Y. Shen, H. Dai, and X. Yang, “Effects of different agricultural organic wastes on soil GHG emissions: During a 4-year field measurement in the North China Plain,” *Waste management,* vol. 81, pp. 202-210, 2018.

[6] Y. Habibi, L. A. Lucia, and O. J. Rojas, “Cellulose nanocrystals: chemistry, self-assembly, and applications,” *Chemical reviews,* vol. 110, no. 6, pp. 3479-3500, 2010.

[7] D. Ciolacu, F. Ciolacu, and V. I. Popa, “Amorphous cellulose—structure and characterization,” *Cellulose chemistry and technology*, vol. 45, no. 1, pp. 13, 2011.

[8] J. Gassan, and A. Bledzki, "Modification methods on nature fibers and their influence on the properties of the composites." pp. 2552-2557.

[9] W. Yueping, W. Ge, C. Haitao, T. Genlin, L. Zheng, X. Q. Feng, Z. Xiangqi, H. Xiaojun, and G. Xushan, “Structures of bamboo fiber for textiles,” *Textile research journal,* vol. 80, no. 4, pp. 334-343, 2010.

[10] M. Yusof, “Properties oil palm frond and kenaf bast fiber by composite tested on different ratio,” University Malaysia Kelantan, 2015.

List of Bibliography (Continued)

[11] W. Fatriasari, M. R. Ridho, A. Karimah, Sudarmanto, Ismadi, Y. Amin, M. Ismayati, M. A. R. Lubis, N. N. Solihat, and F. P. Sari, "Characterization of Indonesian banana species as an alternative cellulose fibers," *Journal of Natural Fibers,* vol. 19, no. 16, pp. 14396-14413, 2022.

[12] S. George, S. Thomas, N. Nandanan Nedumpillil, and S. Jose, "Extraction and Characterization of Fibers from Water Hyacinth Stem Using a Custom-Made Decorticator," *Journal of Natural Fibers,* vol. 20, no. 2, pp. 2212927, 2023.

[13] M. Asrofi, H. Abral, A. Kasim, A. Pratoto, M. Mahardika, J.-W. Park, and H.-J. Kim, "Isolation of nanocellulose from water hyacinth fiber (WHF) produced via digester-sonication and its characterization," *Fibers and Polymers,* vol. 19, pp. 1618-1625, 2018.

[14] B. Shanmugarajah, P. L. Kiew, I. M. L. Chew, T. S. Y. Choong, and K. W. Tan, "Isolation of nanocrystalline cellulose (NCC) from palm oil empty fruit bunch (EFB): Preliminary result on FTIR and DLS analysis," *Chemical Engineering Transactions,* vol. 45, pp. 1705-1710, 2015.

[15] S. Mueller, C. Weder, and E. J. Foster, "Isolation of cellulose nanocrystals from pseudostems of banana plants," *RSC advances,* vol. 4, no. 2, pp. 907-915, 2014.

[16] M. Yu, R. Yang, L. Huang, X. Cao, F. Yang, and D. Liu, "Preparation and characterization of bamboo nanocrystalline cellulose," *BioResources,* vol. 7, no. 2, 2012.

[17] R. M. dos Santos, W. P. F. Neto, H. A. Silvério, D. F. Martins, N. O. Dantas, and D. Pasquini, "Cellulose nanocrystals from pineapple leaf, a new approach for the reuse of this agro-waste," *Industrial Crops and Products,* vol. 50, pp. 707-714, 2013.

[18] K. Pakutsah, and D. Aht-Ong, "Facile isolation of cellulose nanofibers from water hyacinth using water-based mechanical defibrillation: Insights into morphological, physical, and rheological properties," *International journal of biological macromolecules,* vol. 145, pp. 64-76, 2020.

List of Bibliography (Continued)

[19] D. Trache, A. F. Tarchoun, M. Derradji, T. S. Hamidon, N. Masruchin, N. Brosse, and M. H. Hussin, "Nanocellulose: from fundamentals to advanced applications," *Frontiers in Chemistry,* vol. 8, pp. 392, 2020.

[20] K. Phuphantrakun, A. Chandrachai, and S. Ekgasit, "Amorphous Cellulose: Graphene Oxide Composite Bead," *Trends in Sciences,* vol. 20, no. 8, pp. 5496-5496, 2023.

[21] Y. Tong, A.-O. Seibou, M. Li, A. Kaci, and J. Ye, "Bamboo Sawdust as a Partial Replacement of Cement for the Production of Sustainable Cementitious Materials," *Crystals,* vol. 11, no. 12, pp. 1593, 2021.

[22] L. D. Soraisham, N. Gogoi, L. Mishra, and G. Basu, "Extraction and Evaluation of Properties of Indian Banana Fibre (Musa Domestica Var. Balbisiana, BB Group) and Its Processing with Ramie," *Journal of Natural Fibers,* vol. 19, no. 13, pp. 5839-5850, 2022.

[23] P. Garside, and P. Wyeth, "Identification of cellulosic fibres by FTIR spectroscopy-thread and single fibre analysis by attenuated total reflectance," *Studies in conservation,* vol. 48, no. 4, pp. 269-275, 2003.

[24] F. Lionetto, R. Del Sole, D. Cannoletta, G. Vasapollo, and A. Maffezzoli, "Monitoring wood degradation during weathering by cellulose crystallinity," *Materials,* vol. 5, no. 10, pp. 1910-1922, 2012.

[25] A. Y. Melikoğlu, S. E. Bilek, and S. Cesur, "Optimum alkaline treatment parameters for the extraction of cellulose and production of cellulose nanocrystals from apple pomace," *Carbohydrate polymers,* vol. 215, pp. 330-337, 2019.

[26] M. Makarem, C. M. Lee, K. Kafle, S. Huang, I. Chae, H. Yang, J. D. Kubicki, and S. H. Kim, "Probing cellulose structures with vibrational spectroscopy," *Cellulose,* vol. 26, pp. 35-79, 2019.

[27] H. W. Kwak, H. Lee, M. E. Lee, and H.-J. Jin, "Facile and green fabrication of silk sericin films reinforced with bamboo-derived cellulose nanofibrils," *Journal of Cleaner Production,* vol. 200, pp. 1034-1042, 2018.

List of Bibliography (Continued)

[28] P. Shrestha, M. B. Sadiq, and A. K. Anal, "Development of antibacterial biocomposites reinforced with cellulose nanocrystals derived from banana pseudostem," *Carbohydrate Polymer Technologies and Applications,* vol. 2, pp. 100112, 2021.

[29] M. Asrofi, H. Abral, A. Kasim, and A. Pratoto, "XRD and FTIR studies of nanocrystalline cellulose from water hyacinth (Eichornia crassipes) fiber," *Journal of Metastable and Nanocrystalline Materials,* vol. 29, pp. 9-16, 2017.

[30] J. M. González-Domínguez, A. Ansón-Casaos, L. Grasa, L. Abenia, A. Salvador, E. Colom, J. E. Mesonero, J. E. García-Bordejé, A. M. Benito, and W. K. Maser, "Unique properties and behavior of nonmercerized type-II cellulose nanocrystals as carbon nanotube biocompatible dispersants," *Biomacromolecules,* vol. 20, no. 8, pp. 3147-3160, 2019.

[31] D. Bondeson, A. Mathew, and K. Oksman, "Optimization of the isolation of nanocrystals from microcrystalline cellulose by acid hydrolysis," *Cellulose,* vol. 13, pp. 171-180, 2006.

[32] W. Y. Hamad, and T. Q. Hu, "Structure–process–yield interrelations in nanocrystalline cellulose extraction," *The Canadian Journal of Chemical Engineering,* vol. 88, no. 3, pp. 392-402, 2010.

[33] T. Q. Hu, R. Hashaikeh, and R. M. Berry, "Isolation of a novel, crystalline cellulose material from the spent liquor of cellulose nanocrystals (CNCs)," *Cellulose,* vol. 21, pp. 3217-3229, 2014.

[34] E. Syafri, E. Yulianti, M. Asrofi, H. Abral, S. Sapuan, R. Ilyas, and A. Fudholi, "Effect of sonication time on the thermal stability, moisture absorption, and biodegradation of water hyacinth (Eichhornia crassipes) nanocellulose-filled bengkuang (Pachyrhizus erosus) starch biocomposites," *Journal of Materials Research and Technology,* vol. 8, no. 6, pp. 6223-6231, 2019.

List of Bibliography (Continued)

[35] H. C. Oyeoka, C. M. Ewulonu, I. C. Nwuzor, C. M. Obele, and J. T. Nwabanne, "Packaging and degradability properties of polyvinyl alcohol/gelatin nanocomposite films filled water hyacinth cellulose nanocrystals," *Journal of Bioresources and Bioproducts,* vol. 6, no. 2, pp. 168-185, 2021.

[36] B. S. Brito, F. V. Pereira, J.-L. Putaux, and B. Jean, "Preparation, morphology and structure of cellulose nanocrystals from bamboo fibers," *Cellulose,* vol. 19, pp. 1527-1536, 2012.

[37] J. L. Orellana, D. Wichhart, and C. L. Kitchens, "Mechanical and Optical Properties of Polylactic Acid Films Containing Surfactant-Modified Cellulose Nanocrystals," *Journal of Nanomaterials*, 2018.

[38] S.-C. Shi, and G.-T. Liu, "Cellulose nanocrystal extraction from rice straw using a chlorine-free bleaching process," *Cellulose*, vol. 28, no. 10, pp. 6147-6158, 2021.

[39] M. Yu, R. Yang, L. Huang, X. Cao, F. Yang, and D. Liu, "Preparation and characterization of bamboo nanocrystalline cellulose," *BioResources,* vol. 7, no. 2, pp. 1802-1812, 2012.

[40] D. Bondeson, A. Mathew, and K. Oksman, "Optimization of the isolation of nanocrystals from microcrystalline cellulose by acid hydrolysis," *Cellulose,* vol. 13, no. 2, pp. 171, 2006.

APPENDEX A

List of publication

List of Publications

International Journal

1. **Pantamanatsopa, P.**, Ariyawiriyanan, W., & Ekgasit, S. (2022). Production of cellulose nanocrystals suspension with high yields from water hyacinth.
   Journal: Journal of Natural Fibers
   Quartile: Q2 (74th percentile Scopus)
   DOI: https://doi.org/10.1080/15440478.2022.2134266
2. **Pantamanatsopa, P.**, Ariyawiriyanan, W., Sungsanit, K., & Ekgasit, S. (2023). Physicochemical characterization of acid-treated nanocrystal cellulose and amorphous cellulose from bamboo sawdust.
   Journal: Journal of Natural Fibers
   Quartile: = Q2 (74th percentile Scopus)
   DOI: https://doi.org/10.1080/15440478.2023.2286323

International Conference (Proceeding)

1. **Pruttipong Pantamanatsopa,** Warunee Ariyawiriyanan, and Sanong Ekgasit. An Efficient Process for Producing Cellulose Nanocrystals from Banana. The 14th International Polymer Conference of Thailand (PCT-14 Conference). 18-19 July, 2024. Amari Watergate Hotel, Bangkok, Thailand.

APPENDEX B

List of Award and Patent

Award

1. 2021. รางวัลระดับดี จากผลงานเรื่อง “เซลลูโลสนาโนคริสตัลคุณภาพสูงจากผักตบชวาเพื่อการประยุกต์เชิงพาณิชย์” ในการประกวดผลงานนวัตกรรมสายอุดมศึกษา ประจำปี 2564 (มหกรรมงานวิจัยแห่งชาติ 2564; Thailand Research Expo 2021).
2. 2022. รางวัลระดับดีมาก จากผลงานเรื่อง “การพัฒนาการผลิตเซลลูโลสนาโนคริสตัลคุณภาพสูงจากผักตบชวาและขี้เลื่อยไผ่เพื่อการประยุกต์เชิงพาณิชย์” ในการประกวดผลงานสิ่งประดิษฐ์ระดับอุดมศึกษา มทร. ธัญบุรี (The 10th RMUTT Young Talent Innovators Awards 2022).
3. 2023. รางวัลเหรียญทอง จากผลงานเรื่อง “Hyacinth Nanocrystals” ในงานประกวดนวัตกรรม the 48th International Exhibition of Inventions Geneva 2023 ณ เมืองเจนิวา ประเทศ Switzerland.
4. 2023. รางวัลระดับดีมาก จากผลงานเรื่อง “โฟมดูดน้ำมัน” ในงานประกวดผลงานสิ่งประดิษฐ์ระดับอุดมศึกษา มทร.ธัญบุรี
5. 2024. รางวัลเหรียญทอง จากผลงานเรื่อง “R-SORB: A Multi-Function and Highly Efficient Oil Spill Sorbent from Natural Rubber/Cellulose Composite” ในงานประกวดนวัตกรรม “The 17th International Inventions and Innovations Show” (INTARG® 2024) ณ เมืองคาโตไวซ์ สาธารณรัฐโปแลนด์
6. 2024. รางวัลเหรียญทอง จากผลงานเรื่อง “Oil Absorbing Foam” ในงานประกวดนวัตกรรม The 7th China (Shanghai) International Invention & Innovation Expo 2024 ณ เมืองเซี่ยงไฮ้ สาธารณรัฐประชาชนจีน

Patent

1. วารุณี อริยวิริยะนันท์, พฤติพงศ์ พันธมนัสโสภา, และ สนอง เอกสิทธิ์ “กรรมวิธีการสกัดนาโนเซลลูโลสจากผักตบชวา” อนุสิทธิบัตรเลขที่ 23977
2. วารุณี อริยวิริยะนันท์, พฤติพงศ์ พันธมนัสโสภา, สนอง เอกสิทธิ์ “กรรมวิธีการสกัดเส้นใยเซลลูโลสที่มีดัชนีความเป็นผลึกต่ำจากผักตบชวา” อนุสิทธิบัตร เลขที่ยื่น 2401003664 ปี 2567

Biography

Name – Surname	Mr. Pruttipong Pantamanatsopa
Date of Birth	September 06, 1990
Address	Faculty of Engineering, Rajamangala University of Technology Thanyaburi, Pathumthani, 12110
Education	Master's degree material engineering, Faculty of Engineering, Rajamangala University of Technology Thanyaburi
Experiences Work	QA Engineer at Propack industries, Ayutthaya (2012-2013) Design Engineer at Pioneer manufacturing, Ayutthaya (2016-2017)
Telephone Number	089-220-9615
Email Adress	pruttipong_p@mail.rmutt.ac.th